# Lightweight complex metal hydrides for Li-, Na-, and Mg-based batteries

**Matylda N. Guzik[1], Rana Mohtadi[2], Sabrina Sartori[1,a)]** iD

[1]Department of Technology Systems, University of Oslo, Kjeller, NO-2027, Norway
[2]Materials Research Department, Toyota Research Institute of North America, Ann Arbor, Michigan 48105, USA
a)Address all correspondence to this author. e-mail: sabrina.sartori@its.uio.no

Energy density and safety are the main factors that govern the development of the rechargeable battery technology. Currently, batteries beyond typical Li-ion batteries such as those based on solid-state electrolytes (SSEs) or other active elements (e.g., Na or Mg) are being examined as alternatives. For example, SSEs that would enable stable and reliable operation of all-solid-state Li-, Na-, and Mg-based batteries, with preferably improved capacity, are considered to be one of the most desired inventions. Lightweight complex metal hydrides are a family of solid compounds that were recently discovered to have extraordinary ionic conductivities and, in some cases, electrochemical properties that enabled battery reversibility. Consequently, they have become one of the promising electrolyte materials for future development of electrochemical storage devices. In this work, we present an overview of a wide range of lightweight hydride-based materials that could be used as electrolytes and/or anodes for mono-/divalent batteries and have a pivotal role in the implementation of new technological solutions in the field of electrochemistry.

## Introduction

Diversification of energy sources and rapidly growing implementation of renewable options worldwide create new challenges for technological energy storage and conversion solutions. From this perspective, materials that would secure effective implementation of future energy strategies are indispensable. This includes discovery of new compounds with enhanced properties, on the one hand, and reinvestigation of new functionalities of already recognized materials, with well known characteristics, on the other hand.

Electrochemical energy storage in batteries is one of the most important technological solutions in the new energy paradigm. Over the past several decades, nickel-metal hydride (Ni–MH), lead-acid, and Li-ion batteries (LIBs) have triggered a revolution in small personal electronic devices, hybrid, plug-in hybrid, and electric vehicles, and in large-scale stationary applications [1]. However, continuous growth in energy demand and shift into the "green" electricity in the global energy landscape require constant progress on the materials side, which is expected to provide prompt answers to the market needs and ensure implementation of appropriate energy storage options.

The rechargeable LIBs, with reasonably high energy density, reliability, and durability, have become the main players in the commercialized battery technology. A battery consists of two electrodes immersed in an electrolyte. The storage of electrical charge in electrodes occurs via three types of electrochemical reactions: alloying, conversion, and intercalation [2]. The first one offers the highest specific capacity, but it is associated with a large volume change. The conversion reactions involve chemical transformation(s) and are often limited by their irreversibility. Thus, the electrochemical intercalation reactions are the most commonly applied in LIBs. In such a cell, the anode (a negative electrode) is typically made of graphite, while the cathode (a positive electrode) is usually a transition metal oxide, with layered, spinel, or olivine crystal structure. The thermodynamically favored redox reaction allows for reversible transport of $Li^+$ between electrodes, which, in this case, act as ionic intercalation hosts. Magnesium-ion batteries and sodium-ion batteries (NIBs), which recently have been identified as appealing, more element abundant and less expensive alternatives to LIBs, share very similar architectures and are subject of extensive studies expected to accelerate their commercial implementation [2, 3].

Despite the fact that significant improvements in performance of these secondary batteries have been demonstrated, there are still challenges to be addressed. One of them is the identification of new electrolytes that would enable their reliable and safe operation. In LIBs and NIBs, the electrolyte is expected to fulfill higher safety standards than the currently used solvents, characterized by high volatility and flammability. An ideal scenario foresees the integration of a solvent-free and thermally stable inorganic solid-state electrolyte (SSE) into a battery cell [4]. An alternative, cheaper and safer magnesium battery technology—that can provide higher energy capacity—also struggles with the identification of proper electrolytes that, in this case, would support $Mg^{2+}$ insertion in cathodes, ensure efficient and reversible magnesium deposition/dissociation, in addition to being safe and stable toward all battery components [5]. The list of previously explored alternatives spans a broad range of compounds; yet, none of them satisfies the physical, chemical, and electrochemical requirements that a potential electrolyte material for Mg batteries must fulfill.

Hydrides are an important class of compounds and over the years have inspired the development of many practical and environmentally friendly technologies [6, 7]. They have been proven to work in an efficient and a reliable way in many energy-related applications, of which Ni–MH batteries are the most prominent examples. Although the higher requirements in energy density demand in transportation and portable electronics lessened the commercial importance of hydrides, the continuous research in the last decade brought them back into focus by discoveries of novel, latent properties and new potential applications. Complex metal hydrides (CMHs), with the general formula $M_m^{\delta+}[M'H_n]^{\delta-}$, consist of a metal cation ($M^{\delta+}$, in this review, typically lithium, sodium, and magnesium) stabilized by a complex anion $[M'H_n]^{\delta-}$. In lightweight CMHs, the latter is formed by light elements, such as boron ($[BH_4]^-$), aluminum ($[AlH_4]^-$ and $[AlH_6]^{3-}$), or nitrogen ($[NH_2]^-$), coordinated by hydrogen atoms. Over the years, these compounds have been mostly investigated due to their high hydrogen storage capacity [7]. However, recent studies revealed their yet unexplored potential, which goes beyond their original applications [6, 8]. One of the essential new functionalities addresses an integration of lightweight CMHs in rechargeable batteries, either as solid-state/non-aqueous electrolytes and/or electrode materials, and by that opens novel possibilities for broad applications of these compounds in the future electrochemical energy storage technologies.

This review gives a complete overview of up-to-date studies that have focused on the characterization of complex light-metal hydrides with high ionic conductivities as well as examples of their application in rechargeable batteries as electrolytes and/or negative electrode materials. The sections titled "Lightweight CMHs as Li-ion conductors," "Lightweight CMHs as Na-ion conductors," "Conductivity of lightweight CMHs in Mg batteries," and "Conductivity of Li, Na, and Mg ions in 3D boron clusters (*closo*-boranes)" cover literature reports on Li-, Na-, and Mg-ion conductivity in lightweight metal hydride complexes and boron clusters, while in the section titled "Light-metal hydride complexes and 3D boron clusters in rechargeable battery cells: application review," the documented examples of their application in battery cells will be presented. Tables I and II give an overview of the ionic conductivities of the presented lightweight CMHs and selected performance parameters of investigated batteries, respectively.

## Lightweight CMHs as Li-ion conductors
### Borohydrides

The first reported information on ionic conductivity (σ) in hydrides, in the solid-state, dates to the late 1970s (room temperature (RT) mobility of $Li^+$ in $Li_2NH = 3 \times 10^{-4}$ S/cm) [48]. Nonetheless, the interest in this class of materials as fast solid-state ionic conductors has been in focus only recently, driven by the discovery of a high σ value for $LiBH_4$ in 2007 [9]. Since then, the number of studies on ionic conductivities in hydrides has been increasing, with borohydrides and their derivatives being the most intensively investigated compositions. Among numerous advantages that characterize this group of compounds, lightweight, compatibility with Li and Na electrodes, thermal/electrochemical stability, and plasticity, which facilitates manufacturing of an electrolyte/electrode interface, appear as the most appealing.

Nakamori et al. reported that at RT, $LiBH_4$ formed an orthorhombic crystal structure characterized by a low ionic conductivity (approximately $10^{-8}–10^{-6}$ S/cm at 303 K) [10]. However, at 388 K, this low-temperature (LT) modification transformed to the hexagonal high-temperature phase (HT-$LiBH_4$), which revealed a remarkable increase in the Li-ion mobility ($5 \times 10^{-3}$ S/cm at 423 K, Fig. 1 and Table I) [6, 9, 11, 12, 102]. The large band gap reported for both LT-$LiBH_4$ (0.69 eV) and HT-$LiBH_4$ (0.53 eV) suggested a negligible contribution of the electronic conductivity [11, 103, 104]. As such, HT-$LiBH_4$ has qualified as a new solid-state superionic conductor, with a potential application as SSE in LIBs. Later, reports evidenced that the observed increase in the ionic conductivity of $Li^+$ was likely due to rearrangements in the $LiBH_4$ crystal structure. The rotational disorder of the $[BH_4]^-$ units, combined with the formation of metastable interstitial sites and alignment of both the $Li^+$ and $[BH_4]^-$ ions along the *a* and *b* axes permitted for an unhampered migration of $Li^+$ in both directions [11, 105, 106]. In batteries, however, the practical application of the observed phenomena requires stability of the hexagonal HT-$LiBH_4$ at much lower temperatures. To achieve

**TABLE I:** Ionic conductivity (σ) values for reported lightweight CMHs, boron clusters and their anhydrous salts.

| Hydride(s) | σ (S/cm) | T (K) | References |
|---|---|---|---|
| **Li⁺ ion conductors** | | | |
| LiBH$_4$ | $10^{-8}$ | 313 | [9, 10, 11, 12] |
| | $10^{-3}$ | ≥390 | |
| LiBH$_4$ ball milled | $10^{-5}$ | 313 | [13] |
| $(1-x)$Li(BH$_4$) + $x$LiI solid solutions | $10^{-3}$ | 303 | [11, 12, 13, 14, 15] |
| | $10^{-2}$ | 413 | |
| $(1-x)$Li(BH$_4$) + $x$LiBr solid solutions | $10^{-6}$ | 313 | [11, 12, 14, 16] |
| | $10^{-4}$ | 413 | |
| $(1-x)$Li(BH$_4$) + $x$LCl solid solutions | $10^{-6}$ | 312 | [14, 17, 18, 19] |
| | $10^{-3}$ | 384 | |
| Li$_2$(BH$_4$)(NH$_2$) | $10^{-4}$ | 303 | [11, 12, 20] |
| | $10^{-2}$ | 378 | |
| Li$_4$(BH$_4$)(NH$_2$)$_3$ | $10^{-4}$ | 303 | [18, 19, 21] |
| | $10^{-1}$ | 513 | |
| Li$_3$(BH$_4$)(NH$_2$)$_2$ | $10^{-3}$ | 313 | [22] |
| Li$_5$(BH$_4$)$_3$NH | $10^{-6}$ | 303 | [23] |
| LiY(BH$_4$)$_4$ | $10^{-6}$ | RT | [24] |
| LiCe(BH$_4$)$_3$Cl | $10^{-4}$ | 293 | [25, 26] |
| LiGd(BH$_4$)$_3$Cl | $10^{-4}$ | 293 | [25] |
| LiLa(BH$_4$)$_3$Cl | $10^{-4}$/ | 293 | [25, 27] |
| | $10^{-5}$ | | |
| LiLa(BH$_4$)$_3$Br | $10^{-5}$ | 293 | [27] |
| LiLa(BH$_4$)$_3$I | $10^{-5}$ | 293 | [27] |
| Li$_3$MgZn$_5$(BH$_4$)$_{15}$ | $10^{-8}$ | RT | [28] |
| Li$_3$MnZn$_5$(BH$_4$)$_{15}$ | $10^{-8}$ | RT | [28] |
| Cs$_2$LiY(BH$_4$)$_6$ | $10^{-9}$ | 303 | [29] |
| Li$_3$K$_3$Ce$_2$(BH$_4$)$_{12}$ | $10^{-7}$ | 303 | [30] |
| Li$_3$K$_3$La$_2$(BH$_4$)$_{12}$ | $10^{-7}$ | 303 | [30] |
| Sr-doped Li$_3$K$_3$Ce$_2$(BH$_4$)$_{12}$ | $10^{-6}$ | 303 | [30] |
| Eu-doped Li$_3$K$_3$Ce$_2$(BH$_4$)$_{12}$ | $10^{-5}$ | 303 | [30] |
| Eu-doped Li$_3$K$_3$La$_2$(BH$_4$)$_{12}$ | $10^{-5}$ | 303 | [30] |
| LiCa$_3$(BH$_4$)(BO$_3$)$_2$ | $10^{-6}$ | 303 | [31] |
| Na-doped LiCa$_3$(BH$_4$)(BO$_3$)$_2$ | $10^{-5}$ | 303 | [31] |
| Sr-doped LiCa$_3$(BH$_4$)(BO$_3$)$_2$ | $10^{-5}$ | 303 | [31] |
| Li(NH$_3$)BH$_4$ | $10^{-3}$ | 310 | [32] |
| LiBH$_4$ nanoconfined in SiO$_2$ | $10^{-4}$ | 303 | [33, 34] |
| LiBH$_4$–Al$_2$O$_3$ nanocomposite | $10^{-4}$ | 303 | [35] |
| LiBH$_4$–C$_{60}$ nanocomposite | $10^{-5}$ | 298 | [36] |
| | $10^{-3}$ | 413 | |
| LiBH$_4$–Li$_3$N nanocomposite | $10^{-5}$ | 323 | [37] |
| LiBH$_4$–Li$_2$NH nanocomposite | $10^{-6}$ | 323 | [38, 39] |
| | $10^{-2}$ | 373 | |
| 0.75LiBH$_4$–0.25Ca(BH$_4$)$_2$ | $10^{-6}$ | 313 | [40] |
| | $10^{-3}$ | 373 | |
| $x$LiBH$_4$–NaBH$_4$ | $10^{-5}$ | 333 | [41] |
| | $10^{-2}$ | >373 | |
| 2LiBH$_4$–MgH$_2$ | $10^{-6}$ | <373 | [42] |
| | $10^{-2}$ | >373 | |
| LiBH$_4$–NaBH$_4$–$x$MgH$_2$ | $10^{-5}$ | 333 | [43] |
| | $10^{-3}$ | 383 | |
| LiBH$_4$–NaX (X = Cl, I) | $10^{-5}$ | <373 | [44] |
| | $10^{-2}$ | >373 | |
| 90LiBH$_4$–10P$_2$S$_5$ | $10^{-3}$ | 303 | [45] |
| $x$LiBH$_4$–(100 − $x$)0.75Li$_2$S·0.25P$_2$S$_5$ | $10^{-3}$ | RT | [46] |
| Li(BH$_4$)$_3$I–0.75Li$_2$S·0.25P$_2$S$_5$ | $10^{-3}$ | 313 | [47] |
| LiAlH$_4$ | $10^{-9}$ | 300 | [12, 18] |
| | $10^{-6}$ | 393 | |
| Li$_3$AlH$_6$ | $10^{-7}$ | 300 | [12, 18] |
| | $10^{-5}$ | 393 | |
| Li$_3$AlH$_6$–LiI | $10^{-4}$ | 393 | [18] |

*(continued)*

**TABLE I:** Ionic conductivity (σ) values for reported lightweight CMHs, boron clusters and their anhydrous salts. *(continued)*

| Hydride(s) | σ (S/cm) | T (K) | References |
|---|---|---|---|
| Li$_2$NH | $10^{-4}$ | 298 | [21, 48] |
| | $10^{-2}$ | 400 | |
| Li$_2$Ca(NH)$_2$ | $10^{-6}$ | 298 | [49] |
| | $10^{-4}$ | 400 | |
| LiNH$_2$ | $10^{-9}$ | RT | [21] |
| | $10^{-5}$ | 520 | |
| LiNH$_2$–LiI | $10^{-5}$ | 290 | [18] |
| Li$_2$B$_{12}$H$_{12}$ | $10^{-8}$ | 303 | [50, 51, 52] |
| | $10^{-7}$ | 355 | |
| Li$_2$B$_{12}$H$_{12}$ ball milled | $10^{-5}$ | 303 | [50, 51, 52] |
| | $10^{-4}$ | 355 | |
| Li$_2$B$_{12}$H$_{12}$ nanoconfined | $10^{-7}$ | 298 | [53] |
| LiNaB$_{12}$H$_{12}$ | $10^{-6}$ | 313 | [54] |
| | $10^{-1}$ | 823 | |
| LiCB$_{11}$H$_{12}$ | $10^{-1}$ | 403 | [55] |
| LiCB$_9$H$_{10}$ | $10^{-1}$ | 383 | [56] |
| | $10^{-2}$ | 354 | |
| Li$_2$(CB$_9$H$_{10}$)(CB$_{11}$H$_{12}$) | $10^{-6}$ | 243 | [57] |
| | $10^{-2}$ | 350 | |
| **Na⁺ ion conductors** | | | |
| NaY(BH$_4$)$_4$ | $10^{-7}$ | RT | [24] |
| Na$_2$(BH$_4$)(NH$_2$) | $10^{-6}$ | 300 | [12, 58, 59] |
| Na$_3$BH$_4$B$_{12}$H$_{12}$ | $10^{-3}$ | 293 | [60] |
| Na$_3$NH$_2$B$_{12}$H$_{12}$ | $10^{-4}$ | 372 | [61] |
| NaAlH$_4$ | $10^{-10}$ | 300 | [12, 59, 62] |
| Na$_3$AlH$_6$ | $10^{-7}$ | 300 | [12, 59, 62] |
| | $10^{-6}$ | 433 | |
| Na$_2$B$_{12}$H$_{12}$ | $10^{-7}$ | 323 | [63] |
| | $10^{-1}$ | 550 | |
| Na$_2$B$_{12}$H$_{12}$ ball milled | $10^{-4}$ | 313 | [50] |
| | $10^{-1}$ | 550 | |
| Na$_2$B$_{12}$Cl$_{12}$ | $10^{-7}$ | 370 | [64] |
| | $10^{-1}$ | 773 | |
| Na$_2$B$_{12}$Br$_{12}$ | $10^{-8}$ | 400 | [64] |
| | $10^{-1}$ | 873 | |
| Na$_2$B$_{12}$I$_{12}$ | $10^{-7}$ | 370 | [64] |
| | $10^{-2}$ | 873 | |
| Na$_2$B$_{10}$H$_{10}$ | $10^{-2}$ | 383 | [65] |
| Na$_2$B$_{10}$H$_{10}$B$_{12}$H$_{12}$ | $10^{-1}$ | 303 | [50, 66, 67] |
| NaCB$_{11}$H$_{12}$ | $10^{-1}$ | 383 | [55] |
| NaCB$_9$H$_{10}$ | $10^{-1}$ | 373 | [56] |
| | $10^{-2}$ | 297 | |
| Na$_2$(CB$_9$H$_{10}$)(CB$_{11}$H$_{12}$) | $10^{-1}$ | 383 | [50, 57] |
| | $10^{-2}$ | 300 | |
| α-NaCB$_{11}$H$_{14}$ | $10^{-3}$ | 300 | [68] |
| **Mg²⁺ ion conductors** | | | |
| Mg(BH$_4$)(NH$_2$) | $10^{-6}$ | 393 | [69] |
| cis-Mg(en)(BH$_4$)$_2$ | $10^{-8}$ | 303 | [70] |
| | $10^{-5}$ | 343 | |
| Mg(BH$_4$)$_2$–LiBH$_4$ in DGM | $10^{-3}$ | RT | [71] |
| Mg(BH$_4$)$_2$–LiBH$_4$ in TG | $10^{-5}$ | RT | [72] |
| Mg(BH$_4$)$_2$–LiBH$_4$ in DGM/TG | $10^{-3}$ | RT | [73] |
| Mg(BH$_4$)$_2$ in DGM/THFPB | $10^{-3}$ | 298 | [74] |
| Mg(C$_2$B$_{11}$H$_{12}$)$_2$ in TG | $10^{-3}$ | RT | [75] |
| Mg(C$_2$B$_{10}$H$_{11}$)Cl in THF | $10^{-3}$ | RT | [76] |

this goal, various experimental approaches have been implemented.

## Cation and/or anion substitution

Orimo's group, motivated by the studies on the thermal stability of borohydrides [107], performed systematic

**TABLE II:** Selected parameters for reported lightweight CMHs- and boron clusters-based Li-, Na-, and Mg-ion batteries. Values of first/nth discharge capacities and the capacity retention were taken directly from reported publications and given if available.

| Battery anode II cathode/operation temperature (K) | Hydride/role | First discharge capacity (mAh/g) | nth discharge capacity (mAh/g) | Capacity retention (%)/n (number of cycles) | References |
|---|---|---|---|---|---|
| **Li-ion batteries** | | | | | |
| Li II LiCoO$_2$/393 | LiBH$_4$/solid state electrolyte | 89 | 30th/86 | 97/n = 30 | [12, 77] |
| Li II LiCoO$_2$/353 | LiBH$_4$–C$_{60}$ nanocomposite/solid state electrolyte | 10.4 | 5th/~10 | ~96/n = 5 | [36] |
| Li II LiCoO$_2$/323 | Li$_2$B$_{12}$H$_{12}$/solid state electrolyte | ~64 | 5th/~54 | 60/n = 20 | [51] |
| Li II Li$_4$O$_5$O$_{12}$/333 | Li$_4$(BH$_4$)$_3$I/solid state electrolyte | 142 | 10th/110 | 77/n = 10 | [78] |
| Li II Li$_4$O$_5$O$_{12}$–Li$_4$(BH$_4$)$_3$I/296 | Li$_4$(BH$_4$)$_3$I/solid state electrolyte | 122 | 5th/111 | 91/n = 5 | [79] |
| Li II Li$_4$O$_5$O$_{12}$–Li$_4$(BH$_4$)$_3$I/423 | Li$_4$(BH$_4$)$_3$I/solid state electrolyte | 179 | 2nd/158 | 78/n = 100 | [79] |
| Li II LiCoO$_2$–80Li$_2$S·20P$_2$S$_5$/298 | Li$_4$(BH$_4$)$_3$I/solid state electrolyte | 92 | 20th/82 | 90/n = 20 | [19] |
| Li II LiNi$_{1/3}$Mn$_{1/3}$Co$_{1/3}$O$_2$–Li$_3$BO$_3$ without an adhesive layer/423 | Li$_4$(BH$_4$)$_3$I/solid state electrolyte | 56 | 10th/16 | 29/n = 10 | [80] |
| Li II LiNi$_{1/3}$Mn$_{1/3}$Co$_{1/3}$O$_2$–Li$_3$BO$_3$ with the LiBH$_4$–LiNH$_2$ adhesive layer/423 | Li$_4$(BH$_4$)$_3$I/solid state electrolyte | 114 | 10th/81 | 71/n = 10 | [80] |
| Li II S–LiBH$_4$/393 | LiBH$_4$/solid state electrolyte | 1140 | 45th/730 | 64/n = 45 | [81] |
| Li II S/373 | Li$_4$(BH$_4$)$_3$Cl/solid state electrolyte | 1377 | 5th/636 | 46/n = 5 | [82] |
| Li II S/328 | Nanoconfined LiBH$_4$/solid state electrolyte | >3000 | 2nd/1570 | 78/n = 70 | [83] |
| LiIn II S–LiCe(BH$_4$)$_3$Cl/318 | LiCe(BH$_4$)$_3$Cl/solid state electrolyte | 1196 | 9th/510 | 43/n = 9 | [84] |
| Li II TiS$_2$–LiBH$_4$/393 | LiBH$_4$/solid state electrolyte | 80 | 2nd/205 | 88/n = 300 | [12, 85] |
| Li II TiS$_2$–LiBH$_4$/393 | Li$_4$(BH$_4$)$_3$I/solid state electrolyte | 61 | 2nd/216 | 100/n = 15 | [19] |
| Li II TiS$_2$–Li II TiS$_2$–LiBH$_4$/393 | Li$_4$(BH$_4$)$_3$I/solid state electrolyte | 49 | 2nd/141 | 54/n = 15 | [19] |
| LiIn II TiS$_2$/300 | 90LiBH$_4$·10P$_2$S$_5$/solid state electrolyte | 192 | 2nd/228 | 98/n = 10 | [45] |
| Li II TiS$_2$–Li$_4$(BH$_4$)$_3$I–90LiBH$_4$·10P$_2$S$_5$/303 | Li$_4$(BH$_4$)$_3$I–90LiBH$_4$·10P$_2$S$_5$/solid state electrolyte | ~650 | 2nd/~400 | 54/n = 3 | [86] |
| Li II TiS$_2$–LiBH$_4$/353 | Li$_2$B$_{12}$H$_{12}$/solid state electrolyte | 230 | 10th/~205 | 83/n = 20 | [52] |
| Li II TiS$_2$–LiBH$_4$/403 | LiCB$_{12}$H$_{12}$/solid state electrolyte | 240 | 5th/180 | 75/n = 5 | [55] |
| TiH$_2$–LiBH$_4$ II Li/393 | LiBH$_4$/solid state electrolyte | 1225 | 2nd/1094 10th/1035 | 80/n = 50 | [87] |
| MgH$_2$–LiBH$_4$ II Li/393 | LiBH$_4$/solid state electrolyte | 1488 | 93rd/270 | 18/n = 93 | [87, 88] |
| MgH$_2$–LiBH$_4$–Nb$_2$O$_5$ II Li/393 | LiBH$_4$/solid state electrolyte | 1586 | 100th/700 | 44/n = 100 | [87, 88] |
| MgH$_2$–LiBH$_4$–C-nanofiber II Li/393 | LiBH$_4$/solid state electrolyte | 1728 | 3rd/1889 | 59/n = 50 | [89] |
| MgH$_2$–CoO$_2$–LiBH$_4$ II Li/393 | LiBH$_4$/solid state electrolyte | ~1200 | 2nd/~950 | ~58/n = 21 | [90] |
| MgH$_2$ II Li/303 | Li$_4$(BH$_4$)$_3$I–90LiBH$_4$·10P$_2$S$_5$/solid state electrolyte | ~750 | 2nd/~625 | ~89/n = 3 | [86] |
| Mg$_2$FeH$_6$–LiBH$_4$ II Li/– | LiBH$_4$/solid state electrolyte | 1254 | 2nd/~625 | ~24/n = 10 | [91] |
| 0.8MgH$_2$–0.2TiH$_2$–LiBH$_4$ II Li$_2$S–LiBH$_4$/393 | LiBH$_4$/solid state electrolyte | 910 | 25th/780 | 86/n = 25 | [42] |
| Al–LiBH$_4$ II Li/408 | LiBH$_4$/solid state electrolyte | 895 | 2nd/~500 | ~11/n = 10 | [92] |
| Bi$_2$Te$_3$–LiBH$_4$ II Li/– | LiBH$_4$/solid state electrolyte | 550 | … | … | [93] |
| Si–C II Li/353 | LiBH$_4$–C$_{60}$ nanocomposite/solid state electrolyte | 3480 | 2nd/~900 | ~26/n = 2 | [36] |
| Mg(BH$_4$)$_2$ II Li/– | Mg(BH$_4$)$_2$/active anode material | ~520 | 2nd/~600 | … | [94] |
| NaBH$_4$ II Li/– | NaBH$_4$/active anode material | ~212 | 2nd/~225 | … | [94] |
| LiAlH$_4$ II Li/RT | LiAlH$_4$/active anode material | 1180 | … | −n = 1 | [95] |
| Li$_3$AlH$_6$ II Li/RT | Li$_3$AlH$_6$/active anode material | 900 | … | −n = 1 | [95] |
| NaAlH$_4$ II Li/RT | NaAlH$_4$/active anode material | ~1700 | … | … | [96] |
| NaAlH$_4$ II Li/RT | Nanoconfined NaAlH$_4$/active anode material | ~525 | 2nd/440 | 71/n = 20 | [97] |
| NaAlH$_4$ II Li/RT | Nanoconfined NaAlH$_4$/active anode material | … | … | 46/n = 20 | [98] |
| Na$_3$AlH$_6$ II Li/RT | Na$_3$AlH$_6$/active anode material | … | … | … | [96] |
| LiNa$_3$AlH$_6$ II Li/RT | LiNa$_3$AlH$_6$/active anode material | 1872 | … | … | [96] |
| **Na-ion batteries** | | | | | |
| Na II TiS$_2$–Na$_3$NH$_2$B$_{12}$H$_{12}$/535 | Na$_3$NH$_2$B$_{12}$H$_{12}$/solid state electrolyte | … | 2nd/146 100th/102 | 53/n = 200 | [61] |
| Na II NaCrO$_2$/333 | Na(B$_{12}$H$_{12}$)$_{0.5}$(B$_{10}$H$_{10}$)$_{0.5}$/solid state electrolyte | ~88 | 2nd/~87 | 95/n = 20 85/n = 250 | [99] |
| **Mg-ion batteries** | | | | | |
| Mg II Mo$_6$S$_8$/RT | Mg(BH$_4$)$_2$–LiBH$_4$ in DME/nonaqueous electrolyte | 99 | … | 90/n = 300 | [71] |
| Mg II Mo$_6$S$_8$/RT | Mg(BH$_4$)$_2$ in DGM–THFPB/nonaqueous electrolyte | 80 | 100th/70 | 90/n = 600 | [74] |

*(continued)*

**TABLE II:** Selected parameters for reported lightweight CMHs- and boron clusters-based Li-, Na-, and Mg-ion batteries. Values of first/nth discharge capacities and the capacity retention were taken directly from reported publications and given if available. (continued)

| | | | | | |
|---|---|---|---|---|---|
| Mg ‖ Mo$_6$S$_8$/RT | Mg(BH$_4$)$_2$ in TG/nonaqueous electrolyte | 66 | … | … | [72] |
| Mg ‖ Mo$_6$S$_8$/RT | Mg(BH$_4$)$_2$–LiBH$_4$ in TG/nonaqueous electrolyte | 77 | 100th/71 | 92/$n = 107$ | [72] |
| Mg ‖ Mo$_6$S$_8$/RT | Mg(BH$_4$)$_2$–LiBH$_4$ in DGM–TG–PP$_{14}$TFSI/nonaqueous electrolyte | 74 | 3rd/54 | 74/$n = 55$ | [73] |
| Mg ‖ Mo$_6$S$_8$/373 | Mg(BH$_4$)$_2$–PEO–MgO/solid state electrolyte | … | 150th/95 | … | [100] |
| Mg ‖ Mo$_6$S$_8$/RT | Mg(C$_2$B$_{10}$H$_{11}$)Cl/nonaqueous electrolyte | … | 3rd/~93 | 90/$n = 30$ | [76] |
| Mg ‖ Mo$_6$S$_8$/RT | Mg(CB$_{11}$H$_{11}$)$_2$ in TG/nonaqueous electrolyte | ~140 | 10th/~80 | 57/$n = 10$ | [75] |
| Mg ‖ S/RT | Mg(BH$_4$)$_2$ in DGM–THFPB/nonaqueous electrolyte | 956 | 30th/536 | 55/$n = 30$ | [74] |
| Mg ‖ S/423 | Mg(BH$_4$)(NH$_2$)/solid state electrolyte | … | … | … | [69] |
| Mg ‖ FeS$_x$/RT | Mg(BH$_4$)$_2$–LiBH$_4$/nonaqueous electrolyte | … | 50th/350–400 | 50/$n = 200$ | [101] |
| Mg ‖ FeS$_x$/423 | Mg(BH$_4$)(NH$_2$)/solid state electrolyte | … | … | … | [69] |
| Mg ‖ Ag$_2$S/423 | Mg(BH$_4$)(NH$_2$)/solid state electrolyte | … | … | … | [69] |
| Mg ‖ α-MnO$_2$/RT | Mg(CB$_{11}$H$_{11}$)$_2$ in TG/nonaqueous electrolyte | ~170 | 2nd/~125 | 59/$n = 10$ | [75] |
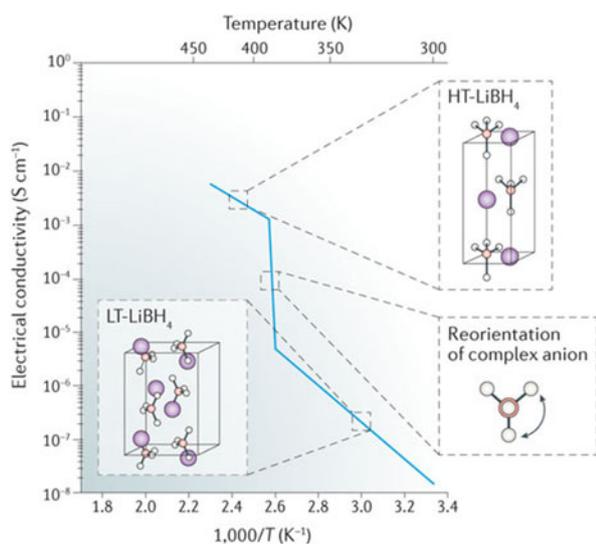


**Figure 1:** The LT-LiBH$_4$ to HT-LiBH$_4$ phase transition triggered by the reorientation of the complex anion with the corresponding Arrhenius plots illustrating changes in ionic conductivity. Reprinted with permission from Ref. 6, copyright 2016 Macmillan Publishers Limited, part of Springer Nature.

investigation of the LiBH$_4$–LiX systems, where a fraction of [BH$_4$]$^-$ was replaced by halide anions (X = Br$^-$, Cl$^-$, and I$^-$) [11, 12, 14, 15]. The $(1 - x)$Li(BH$_4$) + $x$LiI solid solution with a hexagonal crystal structure was successfully obtained by a mechanochemical synthesis (Table I). The replacement of [BH$_4$]$^-$ for I$^-$ stabilized the formation of the HT phase at lower temperatures, which decreased monotonically with an increasing concentration of the I$^-$ ions. As demonstrated by powder X-ray diffraction (PXD), for $x > 13\%$, the HT phase was observed at RT. The sample with 40% of the LiI content

showed σ as high as $0.1 \times 10^{-3}$ S/m and $10 \times 10^{-3}$ S/m at 303 K and 413 K, respectively [11, 12, 13, 14, 15, 108]. Later, it was confirmed that a higher fraction of I$^-$ anions reduced the activation energy and subsequently increased the conductivity of Li$^+$ [109, 110]. On the other hand, the higher mobility of Li$^+$ in Li(BH$_4$)$_{1-n}$I$_n$, compared to LT-LiBH$_4$, was assigned to the I$^-$-induced lattice anharmonicity and the increased distance between neighboring [BH$_4$]$^-$ units [105, 111]. The formation of solid solutions with enhanced Li-ion conductivity was also observed in the LiBH$_4$–LiBr and LiBH$_4$–LiCl systems [14, 16, 17]. Additionally, in the case of Li(BH$_4$)$_{1-n}$Br$_n$, the importance of applied synthesis methods (mechanochemical powder processing alone over combination with thermal annealing) on the ionic transport properties was emphasized [16].

The successful anionic substitution that stabilized the HT-LiBH$_4$ down to RT initiated a broad research activity on LiBH$_4$-related compositions, obtained by either a cation and/or an intermolecular anion substitution.

In 2009, Matsuo et al. reported on the high ionic conductivity of Li$^+$ in trigonal Li$_2$(BH$_4$)(NH$_2$) and cubic Li$_4$(BH$_4$)(NH$_2$)$_3$ borohydride amides, prepared by mechanochemistry. The simultaneous presence of [BH$_4$]$^-$ and [NH$_2$]$^-$ complexes resulted in multiple crystallographic sites for the Li$^+$ cations and increased their mobility to $2 \times 10^{-4}$ S/cm at RT in both compounds [20]. In addition, the study showed that the Li$_2$(BH$_4$)(NH$_2$) activation energy, which is one of the measures of the barriers for lithium-ion migration, decreased from 0.66 to 0.24 eV at 368 K as a result of the compound melting. The σ value in the resulting Li$_2$(BH$_4$)(NH$_2$) ionic liquid reached $6 \times 10^{-2}$ S/cm. For Li$_4$(BH$_4$)(NH$_2$)$_3$, the activation energy was 0.26 eV before melting (513 K) and suggested higher mobility

of Li$^+$ ions than in HT-LiBH$_4$ (0.53 eV) and Li$_2$(BH$_4$)(NH$_2$) [11, 20]. Later, Yan et al. demonstrated that the mechanochemically processed powder mixture of LiBH$_4$ and LiNH$_2$ (molar ratio 1:2) formed cubic Li$_3$(BH$_4$)(NH$_2$)$_2$, isostructural to Li$_4$(BH$_4$)(NH$_2$)$_3$, whose σ was 6.4 × 10$^{-3}$ S/cm at 313 K [22]. Recently, a new orthorhombic Li$_5$(BH$_4$)$_3$NH phase was obtained; however, its lithium ionic conductivity at RT was only 10$^{-6}$ S/cm [23].

LiY(BH$_4$)$_4$ is one of the few bimetallic Li-based borohydrides that has been studied for a potential application as a SSE [24]. This metastable tetragonal phase was synthesized by thermal treatment of ball milled precursors. The significant enlargement of the LiY(BH$_4$)$_4$ unit cell (by 14%), with respect to the constituting components, was assumed to contribute to the relatively high mobility of Li$^+$ cations, which at RT was 1.26 × 10$^{-6}$ S/cm. In 2013, Černý et al. reported on the Li$^+$ ionic conductivity in Li$_3$MZn$_5$(BH$_4$)$_{15}$ (M = Mg, Mn), first trimetallic borhydrides [28]. Their complex crystal structure, which comprises channels built from face-sharing [M(BH$_4$)$_6$] octahedra, raised hope for the high mobility of lithium cations. Unfortunately, the order distribution of Li$^+$ over the crystallographic sites resulted in a low σ, which at RT was only 4 × 10$^{-8}$ S/cm.

A new family of mixed-cation mixed-anion borohydride chlorides, based on Li and rare-earth elements, was discovered in 2012 and later on expanded by other halide analogues (Fig. 2 and Table I) [25, 27]. The LiM(BH$_4$)$_3$Cl series, with M = Ce, Gd, and La, was obtained by the mechanochemical synthesis and subsequent heat treatment of MCl$_3$ and LiBH$_4$ powder mixtures. The PXD studies revealed that the compounds represented a new type of the crystal structure with isolated tetranuclear ionic clusters [M$_4$Cl$_4$(BH$_3$)$_{12}$]$^{4-}$ that were charge-balanced by Li$^+$ cations. LiM(BH$_4$)$_3$Cl were found to be large entropy-stabilized compounds, with the disordered distribution of Li-ions, which boosted the ionic conductivity of compounds. At 293 K, the reported σ values were 1.02 × 10$^{-4}$, 3.5 × 10$^{-4}$, and 2.3 × 10$^{-4}$ S/cm for Ce-, Gd-, and La-containing compounds, respectively. In another study, the series of LiLa(BH$_4$)$_3$X, X = Br, Cl, and I, was synthesized by the addition reaction, which increased the purity of the samples [27]. At 293 K, the ionic conductivity showed the following trend: LiLa(BH$_4$)$_3$Br > LiLa(BH$_4$)$_3$I > LiLa(BH$_4$)$_3$Cl and oscillated around 10$^{-5}$ S/cm. The results indicated a possible influence of the halide size on the mobility of Li-ions. The topological analysis of conduction pathways suggested a channel with two various structural apertures, crossed by Li$^+$ while diffusing through vacancies. The size of these windows narrowed with an increasing size of the halide ion and was optimized for the structure of the bromide-based compound. It was found that the ionic conductivity of LiLa(BH$_4$)$_3$Cl was lower (1.09 × 10$^{-5}$ S/cm) than the values reported earlier, for
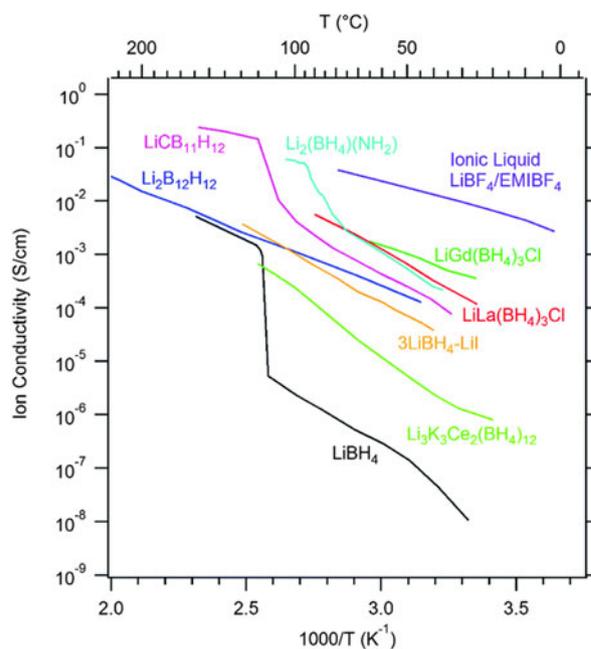


**Figure 2:** Ionic conductivity of Li$^+$ in selected light-metal complex hydrides and boron clusters. Reprinted with permission from Ref. 8, copyright 2017 The Royal Society of Chemistry.

the same compound obtained by a metathesis reaction, and resulted possibly from the percolation effect [112], already observed in mechanochemically processed materials. The study also indicated a correlation between the halide ion type and activation energy, which was the lowest for LiLa(BH$_4$)$_3$I and the highest for LiLa(BH$_4$)$_3$Cl.

The newly discovered bimetallic LiCa$_3$(BH$_4$)(BO$_3$)$_2$ borohydride borate [113] was also reported to have a relatively high ionic conductivity at RT (2.5 × 10$^{-6}$ S/cm) [31]. This number was further increased to 1 × 10$^{-5}$ S/cm for the samples prepared with excess of lithium and doped with either heterovalent Na$^+$ or homovalent Sr$^{2+}$. The presence of extra atoms in the crystal structure did not affect the activation energy values, which indicated the same conduction mechanism in the undoped and doped compositions. The topological analysis suggested that the conduction paths were composed exclusively of BO$_3^{3-}$ anions, which formed face connected tetra- and octahedra accessible for Li$^+$ jumps. The percolating pathway was stabilized by the calcium borohydride substructure, which was not directly involved in the conduction mechanism and indicated vacancy-dependent mobility of Li-ions. LiCa$_3$(BH$_4$)(BO$_3$)$_2$, as a first member of a new family of mixed anion hydrides, has opened possibility for the formation of other hydride-oxide compositions, e.g., SO$_4^{2-}$, PO$_4^{3-}$, or PS$_4^{3-}$.

The investigation of the ionic conduction in borohydrides showed that in this group of compounds, the phenomenon is not exclusively vacancy-dependent and can be explained by a "paddle-wheel" mechanism [26, 114, 115]. It means that in

the crystal structures based on $[M'X_n]^{\delta-}$ polyanions, the fast ionic conductivity is promoted by a high rotational mobility of the $[M'X_n]^{\delta-}$ units, which in turn, decreases the associated activation energy [116].

Owning to a high-density of ionic bonds and packed structures, which are based on coordination polyhedral, metal borohydrides and metal oxides, are very similar. The crystallographic and chemical analogies were successfully used to establish formation rules for perovskite-type metal borohydrides and to predict their physical properties [117]. Disordered complex hydride perovskites may serve as ionic conductors in analogy with oxides such as $La_{2/3-x}Li_{3x}TiO_3$. So far, only limited number of these compounds have been explored for their potential application in electrochemical energy storage solutions. $Cs_2LiY(BH_4)_6$, a trimetallic borohydride, is one of the studied examples [29]. Unfortunately, its cubic double-perovskite crystal structure possesses neither empty crystallographic sites available for $Li^+$ jumps nor conduction channels, with sizes suitable for migration of lithium ions. Thus, at 303 K, its reported σ value was as low as $10^{-9}$ S/cm. The Li-ion conductivity of doped lanthanide-oxide $Li_{3+x}La_3M_2O_{12}$ garnets led to the study on the alkali rare-earth garnet borohydrides, of which $Li_3K_3M_2(BH_4)_{12}$, M = Ce, La, were the first reported examples [30]. Their ionic conductivity at RT, $3 \times 10^{-7}$ and $6 \times 10^{-7}$ S/cm, respectively, was 7 orders of magnitude higher than that of undoped metal oxide garnet analogues. The doping effect of mono- and divalent cations on the Li-ion conductivity in these compounds was also investigated. The results suggested that the presence of $Sr^{2+}$ or $Eu^{2+}$ in Ce- and La-containing compositions increased σ by one order of magnitude in the measured temperature range. Interestingly, to observe this effect, dopant concentrations over four times smaller than in oxides were needed. The enhancement was likely due to changes in the structural dynamics related to the disordering of $[BH_4]^-$ tetrahedra.

The new concept of utilizing reversible ammonia gas sorption in $LiBH_4$ for formation of structural defects, which consequently enhanced the Li-ion mobility, has been recently reported by Zhang et al. (Fig. 3 and Table I) [32, 118]. Solid-state lithium borohydride ammoniates $Li(NH_3)_xBH_4$, x = 0.5 and 1.0, showed a drastic change in the ionic conductivity due to the structural modifications, resultant from the desorption of
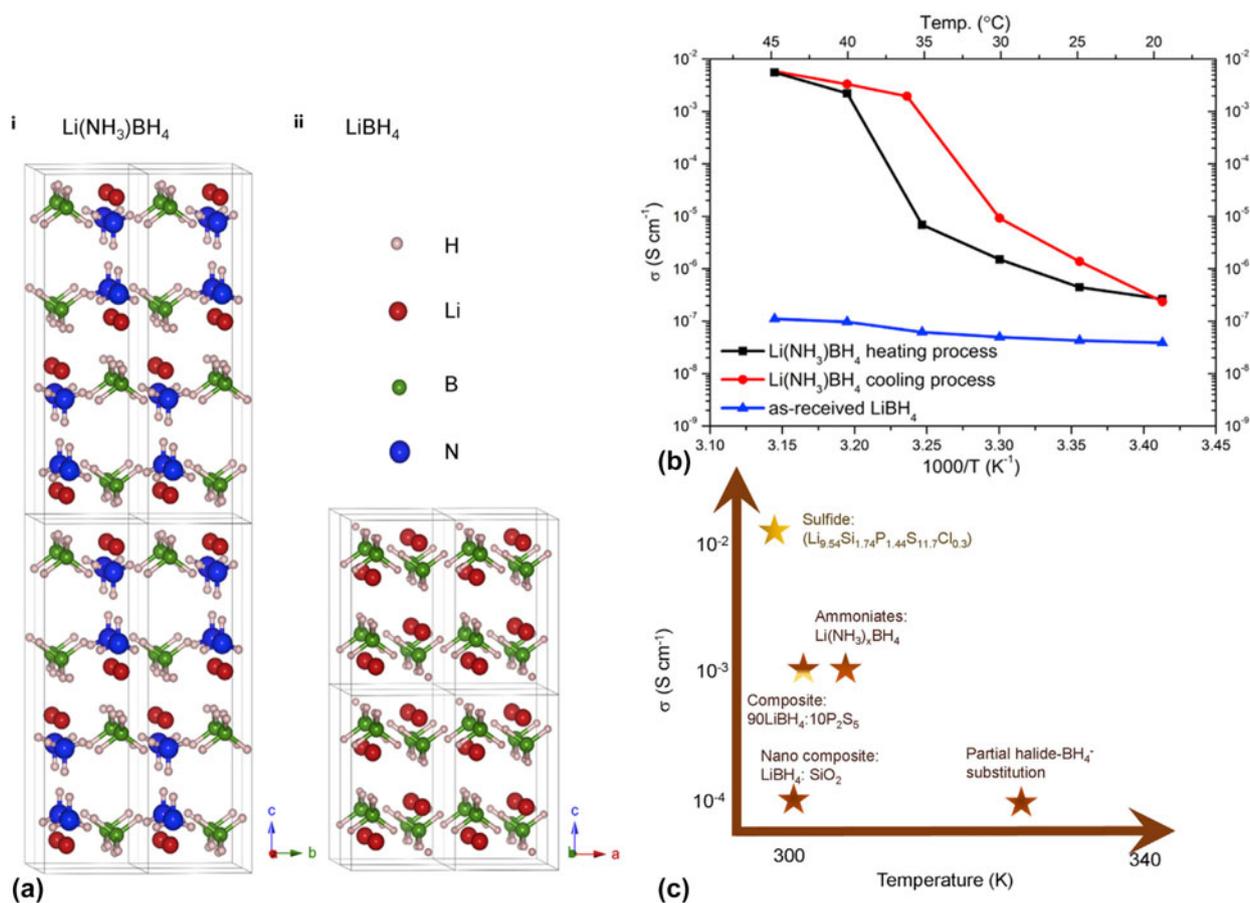


Figure 3: (a) Crystal structures of mono-ammoniate (i) and $LiBH_4$ (ii) with marked unit cells. (b) Li-ion conductivity of $Li(NH_3)BH_4$ during the heating (black) and cooling processes (red). The blue line represents σ of the as-received $LiBH_4$. (c) Status of the ionic conductivity in several borohydride-type electrolytes. Reprinted with permission from Ref. 118, copyright 2018 Elsevier Inc.

$NH_3$. For $Li(NH_3)BH_4$, the $\sigma$ value increased from $1.5 \times 10^{-6}$ S/cm at 303 K to $2.21 \times 10^{-3}$ S/cm at temperatures >313 K, which was associated with the formation of Schottky defects in the compound crystal structure. These new solid-state superconductors were also characterized by a wide electrochemical window (4 V versus $Li/Li^+$).

## Composites

One of the alternative methods promoting the high ionic conductivity in lithium borohydride is the formation of composites with other materials. High $\sigma$ ($10^{-4}$ S/cm) at RT was observed for the $LiBH_4$–$SiO_2$ nanocomposite prepared by melt infiltration of the borohydride into a mesoporous inorganic silica scaffold [33, 119]. Given the high concentration of the insulating $SiO_2$ in the material (up to 50 vol%) and limited stabilization of $HT$-$LiBH_4$ in the matrix pores, the measured ionic conductivity values were surprising. However, the study suggested that the high mobility of $Li^+$ in this case was related to the high density of defects and low diffusion barriers at the interface between two solids, which resulted from disorder, strain, and space-charge regions [33, 120]. The follow up studies on the same system, though synthesized by high energy milling, also demonstrated the fast $Li^+$ diffusion in the obtained materials ($10^{-4}$ S/cm at RT) [34]. This confirmed the importance of the interface-related processes on the enhancement of the ionic conductivity in $LiBH_4$–$SiO_2$. A similar study was later performed on the $LiBH_4$–$Al_2O_3$ system [35]. The results showed that the $Li^+$ ion conductivity of the composite reached $2 \times 10^{-4}$ S/cm at RT and was associated with the formation of a highly defective interface between two solids. Motivated by this discovery, other nano/composites have also been explored. Teprovich et al. reported on fast ionic conduction in the $LiBH_4$–$C_{60}$ system and demonstrated the enhanced mobility of $Li^+$ in the presence of $C_{60}$, which for the mixture with a ratio of 70:30 wt% reached $2.0 \times 10^{-5}$ and $2.0 \times 10^{-3}$ at 298 K and 413 K, respectively [36]. This behavior resulted from the nonionic mechanism, which assumed destabilization of the $Li^+/[BH_4]^-$ ion pairs in the presence of fullerenes.

The high ionic conductivity of polycrystalline $\alpha$- and $\beta$-$Li_3N$ [121] at RT (approximately $10^{-4}$ S/cm for both phases), with however a narrow potential window (<1 V), motivated studies on the $LiBH_4$–$Li_3N$ system [37]. Materials prepared by mechanochemical methods contained crystalline $LT$-$LiBH_4$ and $\beta$-$Li_3N$, and below 380 K, their ionic conductivity was two orders of magnitude higher than unprocessed $LT$-$LiBH_4$ ($10^{-5}$ versus $10^{-7}$ S/cm at 323 K). Although no presence of crystalline intermediate phases was observed, IR studies indicated the formation of N–H chemical bonds. In addition, no occurrence of hexagonal $HT$-$LiBH_4$ was confirmed in the

studied samples. Based on the results, it was concluded that the observed increase in the mobility of $Li^+$ ions was most likely associated with a high defect concentration at the interfaces between crystalline structures and amorphous components. A high $\sigma$ of lithium imide [48] has also attracted attention to the $LiBH_4$–$Li_2NH$ system [38, 39]. The series of borohydride-imide composites prepared with molar ratios 1:1, 1:2, and 1:4 showed ionic conductivities of $10^{-6}$ and $10^{-2}$ S/cm at 323 K and 373 K, respectively [38]. The observed enhancement of the Li-ion diffusion was due to the formation of favorable boundaries by both phases. The increasing concentration of $Li_2NH$ in the system lowered the activation energy in the higher temperature range (373–393 K) but played an opposite effect within the lower temperature zone (323–363 K). In a recent study, the same system showed the formation of a new cavity-rich orthorhombic phase with yet unknown crystal structure [39]. The $\sigma$ values measured for this material oscillated in the same range as in the previous reports and showed the same temperature dependence as the earlier investigated compositions [38].

There are also several reports on the ionic conductivity of $Li^+$ in borohydride–borohydride/hydride composites. A series of $LiBH_4$ and $Ca(BH_4)_2$ powder mixtures were obtained by ball milling [40]. The synthesized materials did not form a bimetallic borohydride. Instead, they consisted of orthorhombic $LiBH_4$, various $Ca(BH_4)_2$ polymorphs, and a small amount of $CaH_2$ that formed upon heating. At 313 K, ionic conductivities of the obtained composites were lower than that of $LiBH_4$ processed in the same way (e.g., $8.8 \times 10^{-6}$ versus $4.6 \times 10^{-5}$ for $0.75LiBH_4$–$0.25Ca(BH_4)_2$ and lithium borohydride, respectively). The increased $\sigma$ was linked to the formation of defects and interfaces upon milling that was likely to open new Li-ion condition pathways. The similar interpretation of the results was given for the mechanochemically processed $xLiBH_4$–$NaBH_4$ powder mixtures [41]. Milling did not cause the formation of a stoichiometric bimetallic borohydride or a solid solution, and the obtained samples consisted of $LT$-$LiBH_4$ and $NaBH_4$. Below the $LiBH_4$ transition temperature, the composites revealed ionic conductivities of one or two orders of magnitude higher than that of pristine $LT$-$LiBH_4$. On the other hand, above 373 K, their $\sigma$ reached $10^{-2}$ S/cm. The result demonstrated that while higher amount of $LiBH_4$ in the mixtures increased the mobility of $Li^+$, the higher fraction of $NaBH_4$ reduced the activation energy values. The ball milled $LiBH_4$–$MgH_2$ composite comprised $LT$-$LiBH_4$ and $MgH_2$ and had 10 times increased mobility of $Li^+$ at temperatures <373 K, as compared with $LT$-$LiBH_4$ [42]. In the follow up study, Xiang et al. investigated mechanochemically processed powder mixtures of $LiBH_4$–$NaBH_4$–$xMgH_2$, with $x = 10$, 20, and 30% [43]. The processed materials consisted of crystalline $NaBH_4$ and $MgH_2$, while the $LiBH_4$ phase was most likely amorphous.

For the LiBH$_4$–NaBH$_4$–30%MgH$_2$ composition, Li$^+$ ion conductivities reached 2.1 × 10$^{-5}$ S/cm and 11.2 × 10$^{-3}$ S/cm at 333 K and 383 K, respectively. Both values were significantly higher than those of LT/HT-LiBH$_4$. The measurements also identified wide potential windows for the studied compositions, ranging from −1 to 4 V (versus Li/Li$^+$), which indicated a high electrochemical stability of the materials. Recently, the ionic conductivities of the LiBH$_4$–NaX (X = Cl, I) composites, obtained by ball milling, were reported [44]. The study showed the presence of the LiBH$_{4-x}$Cl$_x$ halide solid solution and the eutectic LiBH$_4$–NaBH$_4$ composite in the processed LiBH$_4$–NaCl powder mixture. Their coexistence was likely to facilitate the ionic transportation within the system, which below 373 K was greater by 10–100 times than that of LT-LiBH$_4$ and increased to values of 10$^{-2}$ S/cm above 373 K. Much higher conductivity of Li$^+$ at lower temperatures (approximately 10$^{-3}$ S/cm at 300 K) was observed in the crystalline mixture of 90LiBH$_4$–10P$_2$S$_5$ [45]. Thermal heating of the material did not reveal any phase transition which confirmed the composite stability up to 473 K. This new phase was characterized by high plasticity and possessed a wide potential window (0–5 V), which made it suitable for a battery application.

The addition effect of crystalline LiBH$_4$ on the ionic conductivity of sulfide glass electrolytes was also studied [46]. The results showed that a higher content of LiBH$_4$ increased the conductivity of Li$^+$ in the mechanochemically processed mixture of $x$LiBH$_4$–(100 − $x$)0.75Li$_2$S·0.25P$_2$S$_5$. At RT, the composite with $x$ = 33 showed the highest sigma (1.6 × 10$^{-3}$ S/cm) σ and the lowest activation energy (0.30 eV). The Raman spectroscopy results suggested that the state of [BH$_4$]$^-$ incorporated into the sulfide glass matrix was the same as in the HT-LiBH$_4$, with the high rotational freedom and delocalized negative charge. As a consequence, the electrostatic interactions between Li$^+$ and [BH$_4$]$^-$ were weakened, which increased σ values in the obtained glasses. The addition of Li(BH$_4$)$_3$I also enhanced the Li-ion ion conduction of 0.75Li$_2$S·0.25P$_2$S$_5$ [47]. The Li(BH$_4$)$_3$I–0.75Li$_2$S·0.25P$_2$S$_5$ mixture, with a molar ratio of 1:2, revealed σ in the order of 10$^{-3}$ S/cm at RT, with the activation energy of 0.30 eV.

## Alanates

Li-based LiAlH$_4$ and Li$_3$AlH$_6$ alanates is another group of lightweight hydrogen-based materials, investigated in view of their potential application for electrochemical energy storage. These complex hydrides with ionic bonds between Li$^+$ and [AlH$_4$]$^-$/[AlH$_6$]$^{3-}$ are electrical insulators. The Li-ion conductivity of mechanochemically synthesized compounds was reported to increase linearly from 8.7 × 10$^{-9}$ to 4.7 × 10$^{-6}$ S/cm for LiAlH$_4$ and from 1.4 × 10$^{-7}$ to 1.6 × 10$^{-5}$ S/cm for Li$_3$AlH$_6$, when measured from RT to 393 K [12, 18]. Alanates did not

show any jump in the mobility of lithium cations, and the corresponding values of the activation energy were 0.76 and 0.61 eV, respectively. The effect of potential halide ion substitution/presence on the ionic conductivity in Li$_3$AlH$_6$ was also investigated. Ball-milled powder mixtures of Li$_3$AlH$_6$–LiCl and Li$_3$AlH$_6$–LiI, with a molar ratio of 3:1, had σ one and two orders of magnitude higher compared to pure Li$_3$AlH$_6$, respectively. The study also showed the reduction of the activation energy associated with the presence of LiCl and LiI. The likely origin of the observed improvement was associated either with an increased carrier concentration and/or formation of extra vacancies as a result of possible hydrogen substitution by the halide anions [18]. Unfortunately, no follow up studies have been conducted to verify the proposed hypothesis.

## Imides & amides

Li$_2$NH was the first reported hydrogen-based material with the high Li$^+$ mobility at RT (2.5 × 10$^{-4}$ S/cm) [21, 48]. The ionic conduction was mediated by Frenkel pair defects and/or charged vacancies. The cation diffusion occurred via pathways which involved octahedral to tetrahedral jumps along the [001] crystallographic direction. Although, at 400 K, the compound's Li-ion conductivity was as high as 8.40 × 10$^{-2}$ S/cm, poor electrochemical stability (0.7 V versus Li$^+$/Li) hindered its application as a solid-state ionic conductor [21]. The Li-based bimetallic systems with Ca and Mg were also explored [21]. While a high fraction of empty tetrahedral sites in Li$_2$Mg(NH)$_2$ was expected to facilitate the movement of thermally activated ions [49], neighboring Ca[NH]$_6$ octahedral layers in Li$_2$Ca(NH)$_2$ could provide 2D channels necessary for the diffusion of Li$^+$ ions [122]. However, the obtained results did not suggest improved ionic mobility in any of these compounds. At RT, σ for Li$_2$Ca(NH)$_2$ reached only 6.40 × 10$^{-6}$ S/cm, while for Li$_2$Mg(NH)$_2$, it was hardly detectable [21].

The conductivity of Li$^+$ in LiNH$_2$ is much worse than that of Li$_2$NH. The reported value at RT was very low (3 × 10$^{-9}$ S/cm) and at 520 K reached only 2.63 × 10$^{-5}$ S/cm [21]. The theoretical studies on this amide suggested that, even though the Li-ion migration energy was relatively low along different crystallographic directions, defects necessary to mediate the ionic diffusion in the compound were difficult to form, which resulted in low σ. The ionic conductivity was however improved in the LiNH$_2$–LiI system, where the formation of Li$_3$(NH$_2$)$_2$I was observed. The compound was crystallized with the double perovskite structure and its σ was 1 × 10$^{-5}$ S/cm at 296 K [18].

## Lightweight CMHs as Na-ion conductors

The dominance of LIBs on the market naturally shifted the research focus toward solutions, thus compositions, which could improve the current technology. This has not been

different for the hydrides, of which those containing $Li^+$ ions have become the most studied group. However, the recent development in the field of sodium ion batteries (NIBs) sparked the research on the potential electrochemical application of Na-based light-metal hydride complexes [2, 123]. Several Na-based complex hydrides have been investigated, often in parallel to their Li-based analogues; yet, the number of reported cases is very limited. The studied examples of the hydride-based Na-ion conductors also demonstrate that there are still a lot of challenges to be addressed within this emerging technology.

### Borohydrides

The conductivity of $Na^+$ ions in complex hydrides was first studied in the $Na(BH_4)$–$Na(NH_2)$–NaI system [12, 58, 59]. At RT, the σ values for the host materials (e.g., $Na(BH_4)$, $Na(NH_2)$, and NaI) as well as the formed $Na_3(BH_4)_2I$ and $Na_2(NH_2)I$ were very low, in the range of $10^{-10}$–$10^{-9}$ S/m. However, the number increased significantly for $Na_2(BH_4)(NH_2)$ and reached $2 \times 10^{-6}$ S/cm at 300 K. This phase formed by mechanochemical processing of the $Na(BH_4)$ and $Na(NH_2)$ powder mixture, adopted the anti-perovskite cubic $K_3SO_4F$-type structure, which was known to be the HT polymorph [124]. Unlike the nominal $Na(BH_4)I$ and $Na(NH_2)$ I, the crystal structure of $Na_2(BH_4)(NH_2)$ revealed disordered distribution of the $Na^+$ cations, which occupied only 2/3 of the available crystallographic sites. This suggested that the increased mobility of Na ions was vacancy diffusion-dependent. The results also demonstrated the high electrochemical stability of the compound up to 6 V (versus $Na/Na^+$) [12, 58]. Roedern et al. reported on the mobility of the $Na^+$ in bimetallic $NaY(BH_4)_4$ ($6.98 \times 10^{-7}$ S/cm), which at RT was one order of magnitude lower than that of the Li-based analogue [24].

Studies on the superionic conductivity of Na-ions in higher boranes, such as $[B_{10}H_{10}]^{2-}$ or $[B_{12}H_{12}]^{2-}$ [65], suggested that the presence of both $[B_xH_x]^{2-}$ and $[BH_4]^-$ anions in the same crystal structure could stabilize the formation of high-symmetry compounds with the high cationic mobility close to RT. The concept was successfully applied to the $Na_3BH_4B_{12}H_{12}$ mixed-anion borane, whose σ at RT was $0.5 \times 10^{-3}$ S/cm [60], thus comparable to the currently available Na-based superionics, such as β-alumina [125], NASICON [126] or sulfide-based glass ceramics [127]. The 2D ion conduction path involved mixed-anion slabs without $Na_2B_{12}H_{12}$ ones. $Na_3BH_4B_{12}H_{12}$ was stable at RT and showed an electrochemical window up to 10 V (versus $Na^+$/Na) [60]. This study was followed by the discovery of the high $Na^+$ cation mobility in $Na_3NH_2B_{12}H_{12}$, another mixed-anion borane, for which σ = $1.0 \times 10^{-4}$ S/cm, at 372 K. The composition also revealed high electrochemical (10 V versus $Na/Na^+$) and thermal stability (up to 593 K) [61].

### Alanates

Similar to Li-based alanates, mechanochemically synthesized $NaAlH_4$ and $Na_3AlH_6$ were also studied in view of their potential application as SSEs in rechargeable batteries [12, 59, 62]. The results showed that $Na_3AlH_6$ had higher ionic conductivity than $NaAlH_4$, $6.4 \times 10^{-7}$ and $2.1 \times 10^{-10}$ S/cm, respectively. Upon thermal heating, σ for $Na_3AlH_6$ increased up to $4.1 \times 10^{-6}$ S/cm at 433 K. In comparison to their Li-based counterparts, it was demonstrated that hydrides with the $[AlH_6]^{3-}$ complex anion had always higher conductivities than those with the $[AlH_4]^-$ units.

## Conductivity of lightweight CMHs in Mg batteries

The post-lithium-ion battery research has recently shifted focus toward multivalent cations (e.g., $Al^{3+}$, $Ca^{2+}$, or $Mg^{2+}$), which could further increase the energy density of the rechargeable batteries. Magnesium batteries attracted a lot of interest. With high negative potential ($-2.4$ V), high volumetric capacity (3832 mA h/cm versus 2062 mA h/cm and 1136 mA h/cm, for Li and Na, respectively), low cost, and safety, Mg holds very promising properties [2, 3, 6, 20, 59, 69, 71, 128, 129, 130, 131, 132]. As soon as the feasibility of Mg-based electrochemical cells was demonstrated [131], interest in their development has increased rapidly [129, 133, 134, 135]. However, still poor and not fully understood electrolyte performances significantly delay the progress [6, 39, 70, 71, 129, 130, 132, 134]. The simple Mg salts mixed with typical solvents such as propylene carbonate or diethyl carbonate, similar to those used in LIBs, were shown to form a nonconductive layer on the Mg surface and did not allow for the reversible electrodeposition (also known as plating/stripping or deposition/dissolution) of Mg metal [132, 134]. On the other hand, the well-suited electrolytes, based on organohalomagnesium salts and complexes, with high electrochemical stability against oxidation were found to be corrosive due to the presence of chlorides [130, 135]. In 2012, Mohtadi et al. demonstrated the application of $Mg(BH_4)_2$ as a first example of the halogen-free simple salt-type electrolyte in Mg-based batteries [128]. $Mg(BH_4)_2$ in ethereal solvents [i.e., tetrahydrofuran (THF) and dimethoxy-ethane (DME)] enabled the reversible Mg plating/stripping. Interestingly, the addition of $LiBH_4$ to mixed $Mg(BH_4)_2$ and DME increased the current density and Coulombic efficiency to 94%. This was attributed to the higher dissociation of the $Mg(BH_4)_2$ contact ion pair, which led to enhanced presence of $MgBH_4^+$ ions that acted as charge carriers (note that these studies recently inspired using $Ca(BH_4)_2$ in THF to successfully plate/strip Ca metal) [136]. The later study, which expanded the choice of chelatic solvent to diglyme (DGM), demonstrated

the direct relationship between the number of formed electro-donating oxygen sites and the Coulombic efficiency of the corresponding solvated Mg complex electrolytes, which for $Mg(BH_4)_2$–$LiBH_4$ in DGM reached almost 100% [71]. The electrolyte conductivity was $3.27 \times 10^{-3}$ S/cm and the addition of $LiBH_4$, which acted as a second coordination ligand, accelerated the kinetics of the stripping process. Tuerxun et al. reported on the $Mg(BH_4)_2$–$LiBH_4$ electrolyte in tetra-glyme (TG), which enhanced the $Mg(BH_4)_2$ solubility and claimed a widened electrochemical potential window (up to 2.4 V versus $Mg/Mg^{2+}$, note that the high viscosity of TG could mask the decomposition reaction owing to the slow kinetics, thereby artificially expanding the stability) [72]. The reported σ value was $3.8 \times 10^{-5}$ S/cm, and the Coulombic efficiency reached 95%. $Mg(BH_4)_2$–$LiBH_4$ in DGM/TG solvents with the $PP_{14}TFSI$ ionic liquid displayed an ionic conductivity of $3.01 \times 10^{-3}$ S/cm, with a slightly lower Coulombic efficiency (92%), where the observed increased electrochemical stability (3.0 V versus $Mg/Mg^{2+}$) was likely due to sluggish decomposition kinetic effects [73]. In a recent report, the presence of multifunctional additive THFPB in the $Mg(BH_4)_2$DGM (σ = $3.72 \times 10^{-3}$ S/m at 298 K) increased the $Mg(BH_4)_2$ solubility. The electrolyte showed improved current density and an electrochemical stability up to 2.8 V versus $Mg/Mg^{2+}$. It also enhanced the Coulombic efficiency of Mg plating/stripping to 99% [74]. In this case, the reaction of the reductive borohydride with the acidic additive was indicated, thereby partially transforming the borohydride, and therefore, further investigation is needed to identify the new species.

Although the nonaqueous, halogen-free liquid borohydride electrolytes altered the design principles of how Mg metal compatible electrolytes need to look like, stability and safety remain a concern. In addition, the number of suitable SSEs is very limited. Designing solids with sufficiently high magnesium ion conductivity appears challenging due to the divalent positive charge carried by $Mg^{2+}$ cations. Polymer-electrolyte systems, typically based on polyethylene oxide (PEO) and Mg salts, appeared very attractive, but the studies showed incompatibility with the Mg metal anode. In inorganic solids, high Mg conductivity has also been (σ = $10^{-5}$ S/cm) observed but typically at high temperatures (>673 K). However, the successful application of $Mg(BH_4)_2$-based materials as liquid electrolytes, owing to the high reducing stability of the $[BH_4]^-$ anion, has stimulated research on Mg borohydride-based solid-state conductors. So far, only three examples of such materials have been reported. In 2014, Higashi et al. demonstrated enhanced Mg ion conductivity in the $Mg(BH_2)(NH_2)$ ionic salt [69]. This band gap insulator, with σ of $10^{-6}$ S/cm at 393 K, was also characterized by a relatively wide electrochemical window (up to 3 V versus $Mg^{2+}/Mg$). In 2015, Shao et al. reported on the nanocomposite polymer electrolyte based on

PEO, $Mg(BH_4)_2$, and MgO, which allowed for reversible Mg deposition/dissolution with 98% Coulombic efficiency [100]. High values of σ at lower temperatures were recently reported for $cis$-$Mg(en)(BH_4)_2$, en = $NH_2(CH_2)_2NH_2$, by Roedern et al. [70]. The material was obtained by the mechanochemical processing of the ethylene diamine and $Mg(BH_4)_2$ powder mixture. The mobility of $Mg^{2+}$ ions in $cis$-$Mg(en)(BH_4)_2$ increased from $5 \times 10^{-8}$ S/cm to $6 \times 10^{-5}$ S/cm in the temperature range of 303–343 K.

## Conductivity of Li, Na, and Mg ions in 3D boron clusters (*closo*-boranes)

Boron clusters-based salts are known side products that form during the thermal dehydrogenation of borohydrides [7]. Their high thermodynamic stability contributes to partial irreversibility in the hydrogenation of borohydrides, which makes them highly undesirable. In line with the efforts to tackle this challenge, studies aimed at understanding the structural and thermal properties of these salts suggested a potential application of these materials as SSEs [137, 138]. The detailed investigation of the $Li_2B_{12}H_{12}$ structural evolution indicated possible Li-ion conduction following transformation at 638 K to a disordered phase (β phase) with a frustrated $Li^+$ lattice [137]. Solid-state nuclear magnetic resonance (NMR) study of the spin-lattice relaxation in $Na_2B_{12}H_{12}$ salts revealed a substantial increase in the reorientational jump rates of $B_{12}H_{12}^{2-}$, accompanied by fast translational diffusion of $Na^+$ following a first-order transition near 520 K [138]. As discussed in the section Lightweight CMHs as Li-ion conductors, the recent attention to boron hydrogen compounds as SSEs for LIBs was triggered by the discovery of high Li-ion conductivity in the high-temperature phase ($10^{-3}$ S/cm) of complex hydride $LiBH_4$ [9]. These remained the main focus of research until 2014, where interest of examining the thermally stable boron clusters as SSEs (Fig. 2 and Table I) started gaining momentum [6]. This shift occurred concurrent with independent reports of boron clusters as highly performing liquid electrolytes for a rechargeable magnesium battery [76], where in this case icosahedral boron clusters were exploited, owing to their wide electrochemical window and inertness toward Mg metal [5]. In Subsections titled "Hydroborate-based ionic conductors" and "Carbaborate-based ionic conductors," this new family of ionic conductors is discussed.

### Hydroborate-based ionic conductors

The exploitation and demonstration of *closo*-boranes as potential electrolytes for multivalent batteries (i.e., magnesium) was first reported by Carter el al. [76]. The use of the borane clusters was proposed to enable the expansion of the electrochemical window of magnesium borohydride (discussed

earlier), previously shown to possess high compatibility with the Mg metal [5]. One key challenge with the $B_{12}H_{12}^{2-}$ anion was its insolubility in ethereal solvents that could function in Mg batteries, and for that, modifications of the cluster's icosahedron was necessary, as discussed in the section titled "Carbaborate-based ionic conductors." At the same time, the presence of cationic translational mobility in boron clusters was discovered and first reported for $Na_2B_{12}H_{12}$, where the high $Na^+$ ion conductivity in the order of $10^{-1}$ S/cm near 540 K was obtained [63]. These conductivities were observed following the transition from a low-temperature (ordered monoclinic) to a high-temperature (disordered, body centered cubic) phase and were consistent with $^{23}Na$ NMR measurements showing enhancements in the $Na^+$ cation jump rate ($>2 \times 10^8$ jumps/s) in the high temperature polymorph [138]. It was also speculated that the reorientational mobility of the boron clusters could affect the ionic conductivity through the paddle-wheel mechanism, e.g., rapid spinning of $B_{12}H_{12}^{2-}$ accompanied the phase transition. While this fundamental finding was interesting, from a SSE utility point of view, reduction of the transition temperature and enhancements in the cationic conductivities were needed. This was initially attained through shifting to $Na_2B_{10}H_{10}$, where a disordered face centered cubic phase ($>360$ K) allowed for high Na-ion conductivities in the order of 0.01 S/cm at 383 K (Figs. 4 and 5) [65]. It was suggested that, compared to the $B_{12}H_{12}^{2-}$, the less spherical $B_{10}H_{10}^{2-}$ allowed for more free space between anions for the cation diffusion. In any case, boron clusters were thought to allow for the cationic mobility as a result of a large number of $Na^+$ vacancies coupled with a large anion/cation size ratio that was thought to lead to larger interstitial diffusion pathways [63, 65]. These results suggested that the anion dynamics was one major contributor to the conduction of the cation. For example, ab initio molecular dynamics (AIMD) simulations showed that the

$Li^+$ ion diffusivity in $\beta$-$Li_2B_{12}H_{12}$ would be reduced by 3 orders of magnitude if the anion was constrained and immobile [139]. Recently, computational studies have demonstrated that the energy landscape that the cation experiences, which determines its mobility, is not only resultant of the anion dynamics but rather the complex interplay between the anion rotation/vibrations, the density of accessible diffusion sites, and the nature of local bonding [140].

In an effort to enhance the conductivity of the $Na^+$ cations at lower temperatures, other design approaches included partial substitution with another anion such as $[BH_4]^-$ and $X^-$, X = Br, Cl, I, or with a cation like $Li^+$ were applied [54, 60]. In cases where $[BH_4]^-$ was present in the structure, the absence of order-disorder transition hinted that the anion dynamics were less important contributor to the superconductivities and that structural factors were more at play. For example, the conductivity of $Na_3BH_4B_{12}H_{12}$ at RT was $0.5 \times 10^{-3}$ S/cm, which was several orders of magnitudes higher than that of $Na_2B_{12}H_{12}$ [Fig. 4(b)] [60]. Partial substitution of $[BH_4]^-$ with $I^-$ yielded much lower RT conductivities (in the order of $10^{-5}$ S/cm), which increased dramatically above 360 K (0.1 S/cm) [27]. However, a recent report investigating the effect of replacing the hydrogens in the $B_{12}H_{12}^{2-}$ anion with halogens showed that high conductivities, in the order of $10^{-1}$ S/cm, were only achieved at temperatures exceeding 673 K. Restrictions in the cluster's reorientation mobility, caused by increased anion mass and strong bonds to $Na^+$, as a result of directional charge distribution on the halogen atoms, contributed to this behavior [64]. On the other hand, a cationic substitution was reported to enhance the ionic conductivity. $LiNaB_{12}H_{12}$ was shown to have $\sigma$ values 8 times higher than that of $Na_2B_{12}H_{12}$ at 550 K, which was hypothesized to be due to synergistic effects between the two cations [Fig. 4(c)] [54]. Note that in this case, both $Li^+$ and $Na^+$ cations were mobile and with the increase in temperature
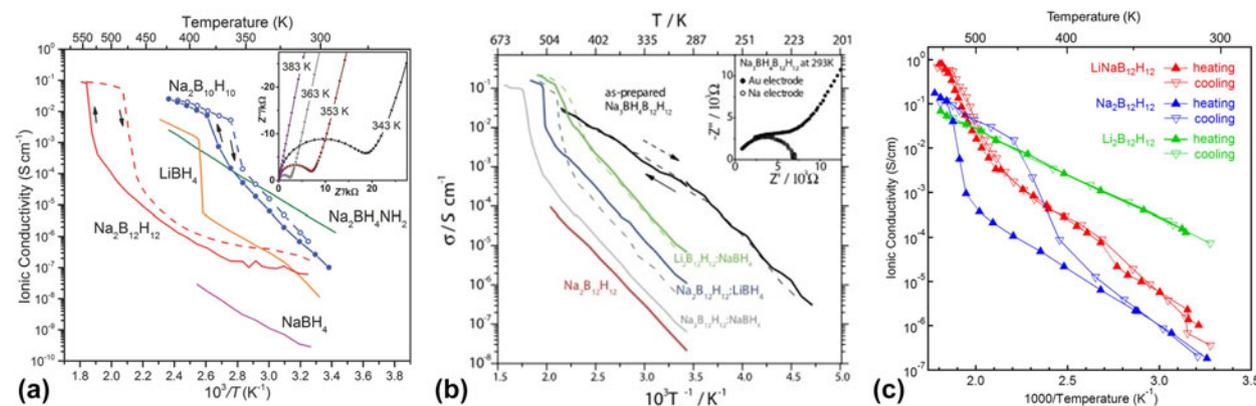


**Figure 4:** (a) T-dependent ionic conductivity of $Na_2B_{10}H_{10}$ compared with other related materials. Reprinted with permission from Ref. 65, copyright 2014 WILEY-VCH. (b) T-dependent ionic conductivity of as-milled $M_2B_{12}H_{12}$: $MBH_4$ (M = Li, Na) and as-prepared $Na_3BH_4B_{12}H_{12}$. Conductivity of the $Na_2B_{12}H_{12}$ precursor is shown for comparison. Reprinted with permission from Ref. 60, copyright 2015 WILEY-VCH. (c) T-dependent ionic conductivity of $LiNaB_{12}H_{12}$, $Na_2B_{12}H_{12}$, and $Li_2B_{12}H_{12}$. Reprinted with permission from Ref. 54, copyright 2015 American Chemical Society.
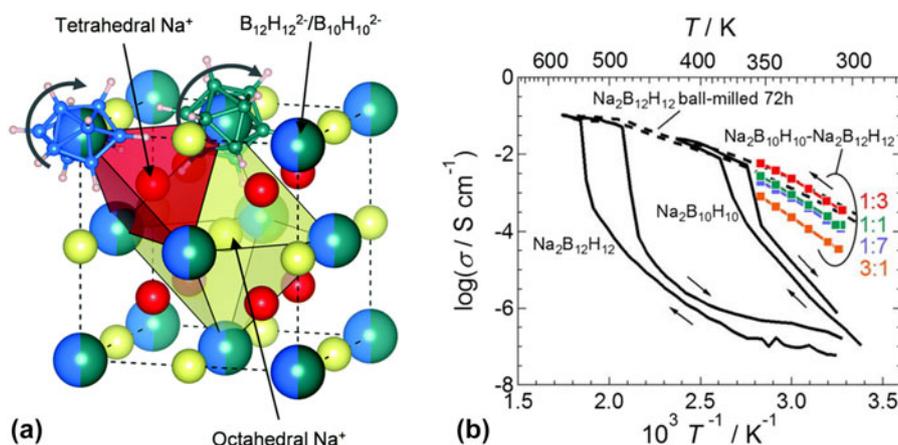
**Figure 5:** (a) Simplified structure of $Na_2B_{10}H_{10}B_{12}H_{12}$ based on the HT phase of $Na_2B_{10}H_{10}$. Partially occupied $Na^+$ ions sites are shown in different colors to distinguish tetrahedral and octahedral coordination. $B_{12}H_{12}^{2-}$ and $B_{10}H_{10}^{2-}$ anions are randomly distributed in the face centered cubic framework. Reprinted with permission from Ref. 66, copyright 2017 The Royal Society of Chemistry. (b) Na-ion conductivity of $Na_2B_{10}H_{10}-Na_2B_{12}H_{12}$ pseudobinary complex hydride with various molar ratios ball milled for 5 h. Different symbols denote the $Na_2B_{10}H_{10}:Na_2B_{12}H_{12}$ molar ratio; 3:1—orange, 1:1—green, 1:3—red, and 1:7—blue. Conductivity data for pristine $Na_2B_{12}H_{12}$ are indicated for comparison. Reprinted with permission from Ref. 67, copyright 2017 AIP Publishing.

from 393 K to 433 K decreased the $Li^+$ transference number from 0.91 to 0.71, respectively. It is however important to point out that the synthetic approach of $LiNaB_{12}H_{12}$ utilized $B_{10}H_{14}$ resulted in the inevitable presence of other cluster fragments such as $B_{10}H_{10}^{2-}$ in the electrolyte, as was shown in $^{11}B$ NMR. This may have inadvertently contributed to the observed improved conductivity. In fact, recently, two independent studies have shown that incorporating $B_{10}H_{10}^{2-}$ in the structure of $Na_2B_{12}H_{12}$ or simply preparing a binary complex of these anions drastically enhanced the $Na^+$ conductivity, e.g., conductivities of 2–3 orders of magnitudes higher than those of $Na_2B_{12}H_{12}$ (Fig. 5) [66, 67].

Beyond the chemical modifications explained earlier, other approaches also sought to improve the cationic conductivity through physical treatments of the material that included the use of mechanochemistry [50, 51]. Ball milling was used initially to briefly condition $Li_2B_{12}H_{12}$ particles, which resulted in ionic conductivity in the order of $10^{-4}$ S/cm at RT. Note that prior to this study, σ measurements for $Li_2B_{12}H_{12}$, following its phase transition at 628 K, were challenging, owing to its thermal instability at these temperatures. It is also important to notice that in the aforementioned approach, $Li_2B_{12}H_{12}$ was prepared from the reaction between decaborane $B_{10}H_{14}$ and $LiBH_4$, which, as explained earlier, produces other cluster fragments that could also contribute to the increase in the conductivity. Thus, this aspect calls for further structural and compositional investigations. Systematic studies of ball milling effects on conductivity improvement in several boron cluster salts were later reported, aided by PXD and Quasielastic Neutron Scattering (QENS). The main finding was that the ball milling effect went beyond particle conditioning, as was evident from the presence of the high temperature disordered phase in the processed materials at RT, which suggested

a stabilized RT disordered form [50]. Conductivity enhancements were drastic, e.g., at RT, the σ value for $Na_2B_{12}H_{12}$ was three orders of magnitude higher than that of the pristine sample. It is interesting that these ball milled solid-state conductors consisted of both the low conducting and superconducting phases. It was hypothesized that the latter was present in a form of the interconnected nanocrystallites that were distributed in larger crystallites, which exhibited typical bulk-like conductivities [50]. Recently, the ball milling effect on $Li_2B_{12}H_{12}$ conductivity (measured in the order of $10^{-5}$ S/cm at RT) was revisited. Unlike previous studies, these improvements were attributed to the formation of not only $Li^+$ but also H deficiencies as was corroborated by theoretical and experimental evidence [52]. In addition, the observed enhancements were suggested to be unlikely related to a stabilization effect of the high temperature phase. Although this was in contrast with the previous report, it was evident from a structural analysis that the lattice parameters were different from those of the high temperature phase, in addition to the preservation of the $Li^+$ structural arrangements. The occurrence of a phase transition to the high temperature disordered phase at 583 K further supported these findings. This study suggested for the first time that deficiencies of H in boron clusters that were stabilized by the cation, could be utilized to improve cationic mobilities, and has opened new opportunities for the design of this type of electrolytes.

Recently, inspired by the dramatic increase in the conductivity of $LiBH_4$ following confinement in a nanoporous silica SBA scaffold, $Li_2B_{12}H_{12}$ was encapsulated in this same scaffold in an attempt to induce similar effects [53]. However, in this case, nanoconfinement of $Li_2B_{12}H_{12}$ was not effective as evident from a very low conductivity compared to that of the bulk material (i.e., $10^{-7}$ S/cm at RT).

## Carbaborate-based ionic conductors

The versatility and rich chemistry of boron clusters prompted investigating the effect of structural modifications on the compounds' electrochemical properties. The first report that demonstrated the uniqueness and applicability of the carbahydroborate anions as electrolytes in multivalent batteries (i.e., magnesium) was reported by Carter et al. [76], where the *m*-dicarborane anion $C_2B_{10}H_{11}^-$ (two of the boron atoms were replaced by two carbons on the 1,7 positions) was used to demonstrate the solubility in ethers magnesium *closo*-borane compound that could efficiently deposit/strip Mg metal. The motivation for using the *closo*-carborane anion was its single charge, which made it less strongly coordinating to the cation compared to its divalently charged $B_{12}H_{12}^{2-}$ counter, in addition to its high anodic stability. This proof of concept was the stepping-stone for the preparation of the Mg salt based on the *closo*-monocarborane anion $CB_{11}H_{12}^-$, known for its high inertness and stability. It was a first demonstration of the simple and halogen-free salt that was compatible with the Mg metal and possessed the widest known electrochemical window amongst Mg electrolytes [75]. This electrolyte has been recognized as the third major breakthrough in Mg battery electrolytes as it overcame major challenges in this battery-type [2].

In case of SSEs, the relatively high σ reported in the hydroborate salts represented an important milestone that highlighted a new potential of boron clusters as SSEs in Li- and Na-based batteries. However, for consideration in practical all-solid-state batteries (SSBs), it is necessary to show whether these high conductivities could be achieved at relevant temperatures. For example, the RT Li-ion conductivities for the sulfide based electrolytes are in the order of $10^{-2}$ S/cm (i.e., 0.025 S/cm for $Li_{9.54} Si_{1.74}P_{1.44}S_{11.7}Cl_{0.3}$) [141], which are orders of magnitude higher than those reported for boron hydrogen compounds [4]. In pursuit of enhancing the cationic mobility in boron clusters, *closo*-carboranes, motivated also by their monovalent charge, Li and Na *closo*-carborane salts were examined [6]. The first report investigated $LiCB_{11}H_{12}$ and $NaCB_{11}H_{12}$ [55]. Similar to other solid-state boron clusters, $LiCB_{11}H_{12}$ and $NaCB_{11}H_{12}$ underwent transition to a superconducting (>0.1 S/cm) disordered phase, however, at much lower temperatures, 400 K and 380 K, respectively (Figs. 2 and 6). The high rate of anion reorientational jumps ($10^{10}$–$10^{11}$ jumps/s), its monovalent charge, and the presence of less neighbors (cation/anion molar ratio = 1:1), coupled with increased lattice constant compared to $B_{10}H_{10}^{2-}$, contributed to the enhanced conductivities. Recent studies, based on both ab initio molecular dynamics (AIMD) and QENS, have confirmed the high reported anion jump rates and showed that this behavior resulted not only from structural factors, such as anion packing or lowering in the anion charge, but also
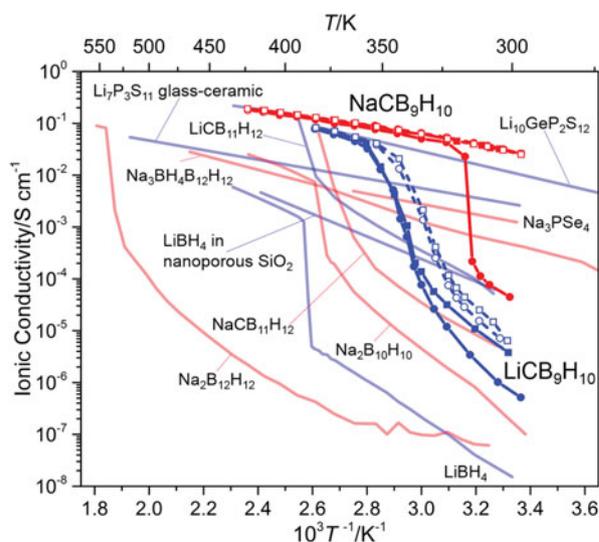


**Figure 6:** Ionic conductivities of boron clusters compared to other electrolytes as functions of inverse temperature. Reprinted with permission from Ref. 56, copyright 2016 WILEY-VCH.

formation of a dipole, which significantly altered the energy landscape of the nearby cations. This frustrated lattice, created by carbon atoms, was suggested to counteract the ability of the phase to order and thereby reduce the transition temperature to superconducting phases [142].

A follow up study examined the lithium and sodium salts of the cage-like anion $CB_9H_{10}^-$ and impressive RT conductivities of about 0.03 S/cm could be achieved in the Na salt but required preheating (i.e., sample conditioning to access the superconducting phase) to about 425 K (Fig. 6) [56]. Note that systematic studies on the effect of the thermal cycling on the RT stability of the disordered superconducting phase are needed to discern the origin of these drastic improvements, especially given the hysteresis observed. For example, long-term stability of RT $Na^+$ conductivity after the first heating cycle is currently unknown. Nonetheless, these findings have qualified the $NaCB_9H_{10}$ salt as the most $Na^+$ conducting SSE reported to date. In addition, substantial improvements were observed for the Li-based salt (Fig. 6), in which conductivities reaching 0.03 S/cm could be achieved at 354 K. Similar to the case of the $NaCB_{11}H_{12}$ and $LiCB_{11}H_{12}$ salts, the dipole produced by the carbon atom could influence the anion orientations and create a frustrated landscape, which was akin to the high cationic mobility.

In an attempt to eliminate the need to preheat $NaCB_9H_{10}$ to achieve the RT high ionic conductivity and to further improve the conductivity of the respective Li-based salt, stabilization of the disordered phase was studied through the formation of what is suggested as mixed as $[CB_9H_{10}CB_{11}H_{12}]^{2-}$ salt [50, 57]. Simple mixing of $CB_9H_{10}^-$ and $CB_{11}H_{12}^-$ Li and Na salts in aqueous solutions resulted in

the presence of the face centered cubic and hexagonal lattice mixtures, which were reminiscent of the disordered phases of the starting material. However, the presence of lattice disorder in both systems prevented detailed structural examination. Ball milling was also used to form the same complexes; however, it was less successful for Li-based salts. In any case, the absence of phase transitions suggested some sort of stabilization effect of the disordered phases at RT. In addition, the reported ionic conductivity of the Li-based salt was surprisingly very high ($6 \times 10^{-3}$ S/cm at 300 K), while the $Na^+$ ion conductivity was very impressive and reached a value of $10^{-2}$ S/cm at 300 K. As the long-term stability of the superconducting phases at RT remains unclear, thermal studies coupled with thorough electrochemical analyses (i.e., anodic/cathodic stability window, impedance evolution) are needed for the carbaborate salts. In addition, battery cycling results are lacking and will be very important in further accessing the potential and challenges of these electrolytes. Similar studies on Na-ion conductivities were extended to other carborane-type derivatives based on several *nido*-carboranes. However, their RT conductivities were inferior to those reported for the *closo*-carboranes (i.e., the highest reported value was for what was described as α-$NaCB_{11}H_{14}$, $10^{-3}$ S/cm at 300 K, it remains unclear why in this case σ was much higher than that in typical $NaCB_{11}H_{14}$, $10^{-6}$ S/cm at 300 K). Although the electrochemical stabilities of these specific salts were not reported, they were expected to exhibit a much narrower window compared to the *closo*-boranes owing to the known limited stability of the *nido*-anions [68].

Just recently, a new report demonstrated the possibility to prepare, for the first time, ionic liquids using *closo*-boranes that remained molten at very low temperatures (i.e., 221 K) [143]. Ionic liquids are molten salts at temperatures below 373 K and offer thermally stable, non-volatile, non-flammable alternative solvents for batteries. They typically consist of an organic cation coupled with an inorganic anion. Formation of ionic liquids that are molten at low temperatures using the *closo*-boron clusters was not previously possible due to the rigid structure of the anion. To compensate for this, the ionic liquids were formed by coupling the *closo*-monocarabrane anion with an ammonium cation that was decorated with flexible alkoxy chains such as $[N_{2(2O,2O1)3}]^+$. The resulting ionic liquid was found to have excellent dissociation and a high conductivity of $10^{-4}$ S/cm at 303 K.

## Light-metal hydride complexes and 3D boron clusters in rechargeable battery cells: application review

The sections titled "Electrolytes in rechargeable Li- and Na-ion batteries," "Electrolytes in rechargeable Mg batteries," and "Interface stability in lightweight complex metal hydride-based all-SSBs" report examples of battery performances, involving the use of light-metal complex hydrides and boron clusters mostly as electrolytes (Table II). Although limited, there also exist exemplifications of the borohydride and alanate applications as negative electrode materials in rechargeable LIBs, as briefly summarized in the section titled "Light-metal hydride complexes as anode active materials in LIBs."

## Electrolytes in rechargeable Li- and Na-ion batteries

The emergence of the lightweight CMHs with high ionic conductivities in the solid-state resulted in exploration of their potential application in rechargeable LIBs and NIBs as SSEs. An acceptable σ value, though indispensable, is one of the crucial electrochemical requirements that must be met by materials to be integrated as SSE into a battery cell. Complex hydrides also possess other technical properties that make them suitable for this type of applications, such as (i) a wide electrochemical window that ensures compound stability in $Li^+$ and $Na^+$ environments; (ii) high mechanical plasticity that enables the formation of good interfaces between battery components and makes battery assembly easy and fast; (iii) high thermal stability as a result of covalent bonding in complex anions; and (iv) low material density (20–50% that of oxides and sulfides), which allows for a higher concentration of the active material and development of the lightweight solutions. Thanks to these characteristics, light-metal hydride complexes have been demonstrated as interesting solid-state alternatives to current liquid electrolytes and contributed to the advancement in the all-solid-state Li- and Na-ion battery technology.

### LIBs

The first example of the $LiBH_4$ application as SSE in all-solid-state battery was reported in 2013 by Takahashi et al. [77]. The compound was tested in an electrochemical cell with Li as an anode and $LiCoO_2$ as a positive electrode. The battery performance was evaluated at 393 K, which ensured the stability of the highly conductive HT-$LiBH_4$ phase. Although SSE showed a high compatibility with the Li electrode, at the same time, the reaction between $LiBH_4$ and $LiCoO_2$ occurred. As a result, a high interfacial resistance was observed, which in turn led to the significant capacity loss. To minimize this effect, an extra layer of amorphous $Li_3PO_4$ was introduced between SEE and the cathode material. This approach improved the battery cycle performance as it retained 97% of the initial discharge capacity (89 mA h/g) after 30 cycles. Sveinbjörnson et al. proposed an alternative approach and showed that coating was unnecessary for a cathode with a lower redox
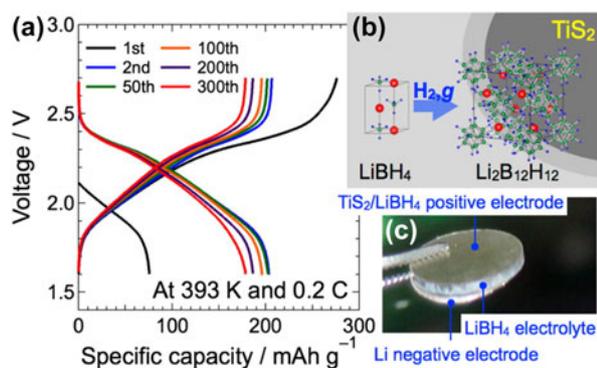
**Figure 7:** Discharge–charge profiles of the bulk-type all-solid-state $TiS_2/Li$ battery operated at 393 K and 0.2C (a). Graphical representation of the $Li_2B_{12}H_{12}$ formation at the $TiS_2/Li$ interface as a result of the chemical/electrochemical reaction between $LiBH_4$ and $H_2$ (b). A photograph of the bulk-type all-solid-state $TiS_2/Li$ battery (c). A part of the Li negative electrode was delaminated for clarity of the battery configuration. Reprinted with permission from Ref. 85, copyright 2015 American Chemical Society.

potential [78]. The study investigated the performance of SSB with $Li_4Ti_5O_{12}$ (LTO) as a positive electrode. Lithium titanite has a redox potential of 1.55 V (versus $Li/Li^+$), which is lower than that of $LiCoO_2$ (3.9 V versus $Li/Li^+$). The application of the $LiBH_4$–LiI solid solution as SSE decreased the cell operation temperature to 333 K. The initial discharge capacity of the battery was 277 mA h/g and accounted for 81% of a LTO theoretical value. This was comparable with the results obtained for the same battery with a liquid electrolyte. Although the all-solid-state battery delivered the discharge capacity above 110 mA h/g (65% of a LTO utilization ratio) during the initial 10 cycles, its discharge capacity retention was worse than that of the liquid electrolyte counterpart. The increased resistance in the SSB cell, due to insufficient contact between SSE and LTO and/or formation of a passivation layer at their interface, was blamed for the observed capacity loss. In a later study, Yoshida et al. replaced the pure LTO cathode with a composite electrode, which consisted of homogeneously dispersed $LTO/Li_4(BH_4)_3I$ with conductive carbon additives [79]. The highly deformable nature of the $Li_4(BH_4)_3I$ SSE resulted in the formation of a tight interfacial contact with the cathode and resulted in the stable battery operation in the range of 296–423 K. At the highest temperature, the battery delivered discharge capacities of 170 and 158 mA h/g, during the first and second cycles, which corresponded to 97% and 90% of a LTO utilization ratio, respectively. The battery capacity retention at this temperature was also very high, and after 100 cycles, it accounted for 140 mA h/g. At 296 K, the battery delivered 122 mA h/g during the initial discharge and its capacity retention was 91% after the fifth cycle. Regardless of the operation temperature, the Coulombic efficiency was nearly 100%, which indicated that the charge–discharge cycling proceeded without side reactions. A smooth operation of the

cell was possible due to very limited charge transfer resistance at the SSE/cathode interface, resulting from a tight contact among electrode constituents. The successful demonstration of the all-solid-state LIB with $Li_4(BH_4)_3I$ at RT (298 K) was also reported by Unemoto et al. The cell comprised the $LiNbO_3$-coated $LiCoO_2$ and $80Li_2S\cdot20P_2S_5$ (LPS) composite electrode, and the Li anode [19]. At the C-rate of 0.1, the discharge capacity was reduced from 92 to 82 mA h/g between the 1st and 20th cycle and the capacity retention was 90%. Although the Coulombic efficiency was only 75% in the initial cycle, it recovered to almost 100% after the second one. The stable and repeated battery operation was possible exclusively by combining SSE electrolytes with different electrochemical stabilities. Another example of the application of $Li_4(BH_4)_3I$ as SSE in LIB was reported by Suzuki et al. [80]. The tested battery consisted of a composite cathode, with $LiNi_{1/3}Mn_{1/3}Co_{1/3}O_2$ (NMC) as an active material and $TiO_2$-doped $Li_3BO_3$, to avoid a direct contact between NMC and SSE. An additional $LiBH_4$ + $xLiNH_2$ ($x$ = 1, 2) adhesive layer was introduced between the positive electrode and $Li_4(BH_4)_3I$. $LiBH_4$ + $xLiNH_2$ has been reported to have the high Li-ion conductivity and a melting temperature of 323 K. Thus, by removing the surface roughness and imperfections, the compound was expected to improve the interface compactness and suppress the contact resistance. The study performed at 423 K demonstrated that the presence of the adhesive layer increased the first discharge capacity from 56 mA h/g to 114 mA h/g, in battery without and with $LiBH_4$ + $xLiNH_2$, respectively. However, it also increased the initial charge capacity above the theoretical value (234 mA h/g versus 115 mA h/g), which suggested the occurrence of side reactions. The presence of the adhesive layer also improved the cycling performance as the capacity retention increased from 29% to 71% for the battery without and with $LiBH_4$ + $xLiNH_2$, respectively.

The feasibility of HT-$LiBH_4$ as SSE was also tested in the lithium–sulfur (Li–S) conversion batteries, characterized by high energy density [81]. To enhance the electrochemical activity of insulating elemental S, a composite S/$LiBH_4$ cathode with conductive carbon (C) was prepared by ball milling. The results demonstrated stable battery operations at 393 K and underlined the important role of borohydrides' ductility, which ensured a good contact at the SSE–cathode interface, obtained exclusively by cold-pressing. The proposed Li–S cell configuration delivered 1140 mA h/g at the rate of 0.05C, during the first discharge, which corresponded to 70% of a sulfur utilization ratio. Over the next 45 cycles, the discharge capacity remained as high as 730 mA h/g with nearly 100% Coulombic efficiency. The Li–S battery operation with the S/C composite cathode was also evaluated with the $LiBH_4$–LiCl solid solution as SSE [82]. The homogeneous dispersion of the electrode constituents ensured a very good SSE/electrode contact and

allowed for the reversible battery operation at 373 K, with the discharge capacity of 1377 mA h/g and 636 mA h/g during the initial and the fifth cycle, respectively. To further lower the operation temperatures of batteries, Das et al. applied nano-confined LiBH$_4$ as SSE in the Li–S cell [83]. The battery containing S/C and Li as positive and negative electrodes, respectively, was evaluated at 328 K and various charge–discharge rates (0.03–0.12C). At higher C-rates, a higher drop of the C/S electrode potential was observed, which obstructed the efficient sulfur utilization. However, by lowering the discharge rate, a quick recovery of the full capacity was obtained. Over 40 cycles, the cell showed good performances and maintained the discharge capacity as high as 1220 mA h/g at 0.03C. Lithium borohydride SSE demonstrated high compatibility also with an all-solid-state metal hydride–sulfur LIB [42]. The cell with Li$_2$S/LiBH$_4$ as a cathode, 0.8MgH$_2$–0.2TiH$_2$/LiBH$_4$ as an anode, and LiBH$_4$ as SSE was operated at 393 K. The reversible specific capacity reached 910 mA h/g, and after 25 charge–discharge cycles, the battery retained 85% of the initial capacity value.

Recently, the stability of LiCe(BH$_4$)$_3$Cl as SSE in a Li–S battery was investigated [84]. The compound was tested in a cell with a S/LiCe(BH$_4$)$_3$Cl composite as a positive electrode and the LiIn alloy as the negative one. The reversible reaction between Li and S was observed at 318 K and a rate of C/100. Although the capacity of the initial discharge and charge reached 1196 mA h/g (71% of the theoretical value) and 879 mA h, respectively, subsequent cycling resulted in significant capacity loss. Still, the capacity retention was satisfactory with the discharge capacity of 510 mA h/g after the ninth cycle.

Much better results and a stable interface formation between the HT-LiBH$_4$ SSE and the active cathode material were reported for the TiS$_2$–Li cell (Fig. 7 and Table II) [12, 85]. A solid-state battery with a TiS$_2$/LiBH$_4$ composite positive electrode, LiBH$_4$ and Li, as the electrolyte and the anode, respectively, was successfully cycled 300 times at 393 K and a rate of 0.2C. Although the initial discharge capacity was only 80 mA h/g (versus 239 mA h/g of the theoretical value), at the second cycle, the parameter reached 205 mA h/g with 100% Coulombic efficiency. This corresponded to 85% of a TiS$_2$ utilization ratio. The battery did not reveal significant capacity fading and during the final discharge the cell delivered 180 mA h/g with the same Coulombic efficiency as in the second cycle. This good durability was explained by the chemical/electrochemical oxidation of the borohydride just below the TiS$_2$ surface. This was accompanied by the hydrogen release and the new phase formation, most likely Li$_2$B$_{12}$H$_{12}$, with high ionic conductivity. The compound revealed high oxidative stability toward LiBH$_4$ and a charge transfer reactivity with the Li anode and as such was likely to act as a stable interfacial layer that enabled numerous charge–discharge cycles.

The oxidative stability of Li$_4$(BH$_4$)$_3$I as SSE was evaluated based on the performance of TiS$_2$–Li batteries with the TiS$_2$/LiBH$_4$ and TiS$_2$/Li$_4$(BH$_4$)$_3$I composite electrodes [19]. Both cells were tested at 393 K with the discharge–charge rate of 0.05C. Similar to HT-LiBH$_4$, the I$^-$-substituted LiBH$_4$ preserved the high mechanical plasticity, which ensured the formation of a robust and tight SSE/cathode interface. Due to the self-discharge reaction and formation of Li$_x$TiS$_2$, the initial discharge capacity of the TiS$_2$/LiBH$_4$-based battery was 61 mA h/g but recovered to 216 mA h/g in the second cycle. On the other hand, the first charge capacity reached 419 mA h/g, which was far above the theoretical value and resulted from the oxidative decomposition of unreacted lithium borohydride. The battery was characterized by a high capacity retention (20 mA h/g) after the 15th cycle. In the cell with the TiS$_2$/Li$_4$(BH$_4$)$_3$I electrode, the first discharge capacity was only 49 mA h/g and recovered to 141 mA h/g during the second cycle. This low initial capacity value was due to the reaction between TiS$_2$ and Li$_4$(BH$_4$)$_3$I, which caused the battery self-discharge prior testing. Over the next 15 cycles, the cell capacity dropped significantly, which was correlated with the steady increase in the internal battery resistance and the lower interface stability between TiS$_2$ and Li$_4$(BH$_4$)$_3$I than between TiS$_2$ and LiBH$_4$. The integration of the crystalline 90LiBH$_4$·10P$_2$S$_5$ (LPS) mixture as SSE in the TiS$_2$–Li battery allowed for its reversible operation at 300 K [45]. The battery was tested against the InLi alloy anode and operated at the C-rate of 0.1. The first and second discharge capacity reached 192 and 228 mA h/g, respectively. After the 10th cycle, the capacity retention was 98% with almost 100% Coulombic efficiency. Recently, a mixture of Li$_4$(BH$_4$)$_3$I and LPS was utilized as SSE in the same battery type [86]. The TiS$_2$/Li$_4$(BH$_4$)$_3$I–LPS composite electrode was tested with the Li$_4$(BH$_4$)$_3$I–LPS electrolyte and Li as a counter electrode at 303 K. The results demonstrated the high compatibility of this SSE mixture toward the electrochemically active materials. The capacity of the initial discharge corresponded to 89% of the theoretical one. The lower C-rate ensured better battery cyclability with a higher Coulombic efficiency.

As soon as metal hydrides and complex transition metal hydrides were proposed as conversion-type anode materials in LIBs, due to their high theoretical Li storage capacity, low volume expansion, and suitable working potential, the possibility of designing SSB with LiBH$_4$ as SSE has been explored [6, 144, 145]. It has been shown that electrochemical performance of the MgH$_2$- and TiH$_2$-based composite electrodes was much better with LiBH$_4$ as SSE than with conventional organic liquid electrolytes [87, 88, 90]. The results for LIB with the TiH$_2$/LiBH$_4$ composite electrode, operated at 393 K, showed that the Li insertion capacity faded little, from 1094 to 878 mA h/g between the 2nd and 50th charge–discharge cycle [88]. For
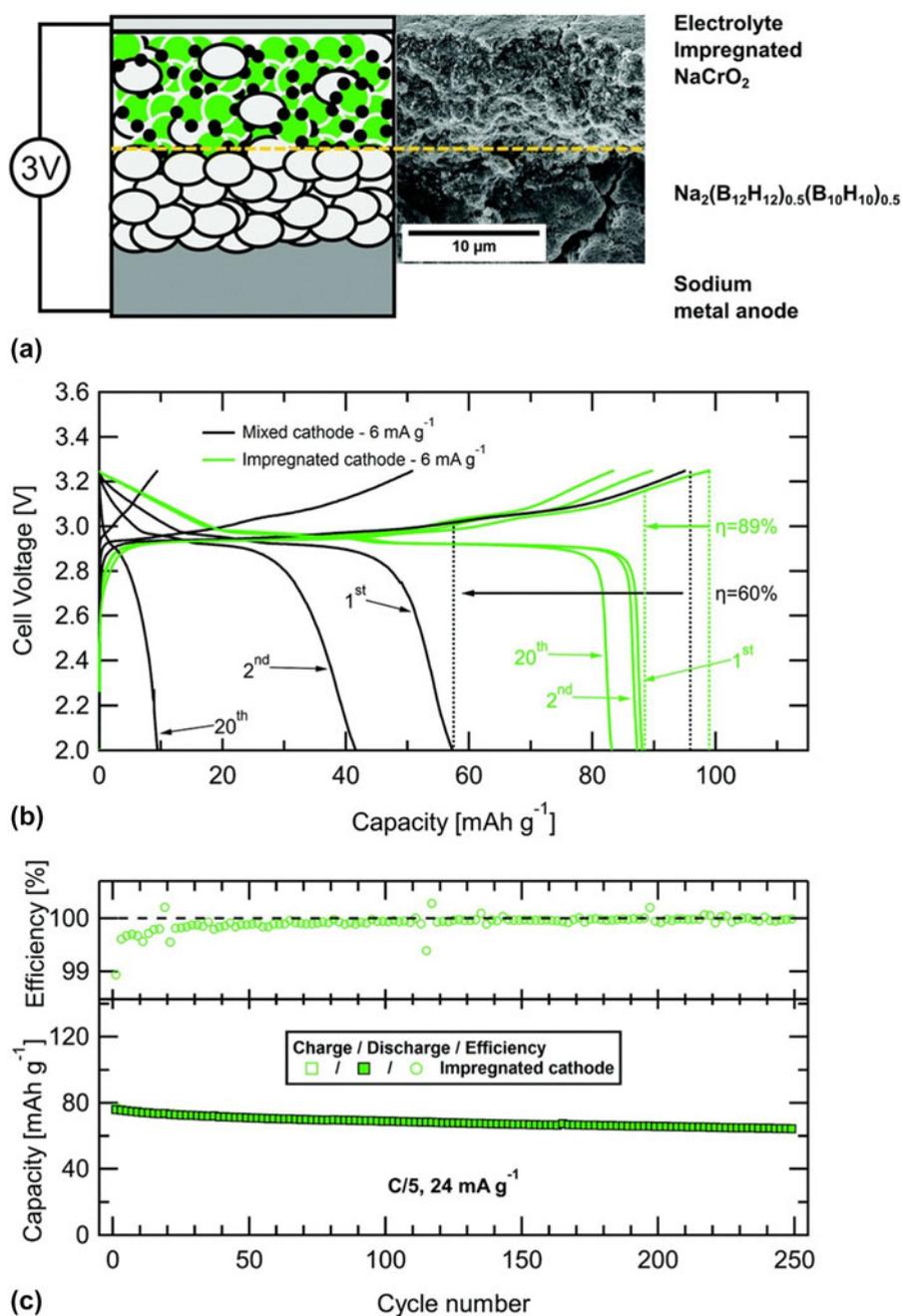
**Figure 8:** (a) Schematic and SEM cross sections of the device investigated in the 3 V Na battery showing the different components of the cell. (b) Charge/discharge profiles for the 1st, 2nd, and 20th cycle of Na|Na$(B_{12}H_{12})_{0.5}(B_{10}H_{10})_{0.5}$|NaCrO$_2$ cells with mixed and impregnated cathode mixtures. (c) Long term cycling of a cell using the impregnated cathode. The cell was initially activated by 3 charge/discharge cycles at 0.05C and subsequently cycled 250 times at 0.2C. Charge and discharge capacity and efficiency are shown every 2 cycles. Reprinted with permission from Ref. 99, copyright 2017 The Royal Society of Chemistry.

SSB with the composite MgH$_2$/LiBH$_4$ and MgH$_2$/LiBH$_4$/Nb$_2$O$_5$ anodes, the initial discharge capacity was 1575 mA h/g and 1650 mA h/g at the C-rate of 0.8, which corresponded to 94% and 95% Coulombic efficiency, respectively. The reported numbers were lower than the theoretical value (2038 mA h/g), but much higher than those obtained for their counterparts with the liquid electrolyte. In addition, both SSBs had improved cyclic stability and better capacity retention. The battery with

the carbon nanofiber supported MgH$_2$/LiBH$_4$ electrode and LiBH$_4$ SSE was also reported to perform better than the same battery with LPS glass-type SSE [89]. The battery with LPS delivered an initial discharge capacity of 1214 mA h/g; however, within next 15 cycles, the value dropped rapidly to only 100 mA h/g. The first charge capacity reached only 575 mA h/g. In comparison, the battery with LiBH$_4$ SSE showed an initial discharge capacity of 1728 mA h/g (94%

Coulombic efficiency), which faded slowly with the increased cycle numbers and remained as high as 1017 mA h/g (99.5% Coulombic efficiency) after 50 cycles [89]. The suitability of $LiBH_4$ as SSE was also demonstrated for all-solid-state LiB with the $MgH_2/CoO_2$ composite electrode [90]. The studies concluded that in this battery-type, solid $LiBH_4$ promoted the hydride conversion reaction due to its dual effect on the $Li^+$ and $H^-$ conductivity. Additionally, a crucial role of the specific anode/electrolyte interface on the reaction kinetic was suggested [87, 88, 89]. Recently, the RT performance of conversion-type $MgH_2$ anode with a mixture of $Li_4(BH_4)_3I$ and LPS as SEE, and lithium as a counter electrode, was reported and compared with the liquid electrolyte cell [86]. The liquid electrolyte-based battery showed higher discharge capacity, but SSB demonstrated a higher reversibility yield. Another recent example of the $LiBH_4$ SSE application in hydride-based LiBs was reported for the $Mg_2FeH_6$-based conversion type anode [91]. In comparison to a cell with a liquid electrolyte, this SSB exhibited a higher value of the initial discharge capacity, 1254 versus 1100 mA h/g, and significantly better Coulombic efficiency, 68 versus 27%. Also, after the 10th cycle, the retained capacity of the cell with the SSE electrolyte was above 3 times higher than that of the conventional counterpart.

The application of $LiBH_4$ as SSE was reported for all-solid-state LIB with an aluminum composite anode (Al/$LiBH_4$) [92]. The cell operated at 408 K and the C-rate of 0.1 revealed the reversible capacity of 895 mA h/g during the initial cycle, which was close to the theoretical value (993 mA h/g). However, subsequent cycling of the material led to a significant capacity loss. Evaluation of the results obtained for charge–discharge cycles at various C-rates indicated that lithium borohydride could facilitate the reversible lithiation of aluminum up to 1C.

Recently, lithium borohydride as SSE was used in a battery cell with a nanostructured $Bi_2Te_3/LiBH_4$ composite anode and Li as an active cathode material [93]. The electrochemical performances of SSBs with $Bi_2Te_3$ nanoparticles and nanosheets were tested. The initial discharge–charge capacities at a rate of 0.1C were 550 mA h/g and 540 mA h/g for nanoparticles and nanoplates-based batteries, respectively.

The suitability of the $LiBH_4$–$C_{60}$ nanocomposite as SSE in all-solid-state LIB was tested in a cell with a silicon/conductive carbon anode and the Li cathode, at 353 K and C-rate of 0.1C [36]. The first discharge capacity reached 91% of the theoretical value (4200 mA h/4 for $Li_{4.4}Si$); however, only two charge–discharge cycles were performed due to the significant performance degradation. This was attributed to the conductivity loss in Si as a result of its large volume expansion upon cycling. The same SSE was also tested in

a cell with $LiCoO_2$ and Li, as a cathode and an anode, respectively [36]. The battery was cycled five times with a rate of 0.1C at 323 K and 353 K. The reversible capacity values reached only 8 and 10 mA h/g, respectively, and were explained by either poor contacts between SSE and the active material and/or side reactions between the electrolyte and $LiCoO_2$.

Battery demonstrations were also reported for boron cluster-based electrolytes using different cathodes. These included battery cycling in H/B deficient $Li_2B_{12}H_{12}$ at 353 K, where the Li metal anode and $TiS_2$ (voltage approximately 2.6 V) were the negative and positive electrodes, respectively [52]. The battery was cycled at low rates (0.05C) and showed a gradual capacity fade. The $TiS_2$ cathode was also used to demonstrate the performance of the $LiCB_{11}H_{12}$ battery operated at 403 K and the C-rate of 0.2. As for $Li_2B_{12}H_{12}$, also in this case, capacity fading was observed (i.e., the capacity dropped from 240 to 180 mA h/g by the fifth cycle). Batteries were also examined with higher voltage cathodes. The ball milled $Li_2B_{12}H_{12}$ was used in a $Li/LiCoO_2$ cell, which was run at 323 K and a rate of 0.2C. However, only 40% of the initial capacity was obtained by the 20th cycle.

## Na-ion batteries

The $Na_3NH_2B_{12}H_{12}$ complex hydride, obtained from metal amide and higher borane, has been recently employed as SSE in the all-solid-state NIB, with the composite $TiS_2/Na_3NH_2B_{12}H_{12}$ cathode and the Na anode [61]. The cell was reversibly operated at 535 K and a rate of 0.1C, over 200 cycles. During the second discharge, the battery delivered 146 mA h/g with almost 100% Coulombic efficiency, which indicated no significant side reactions. After 100 cycles, the capacity retention was as high as 102 mA h/g and dropped to 77 mA h/g during subsequent 100 cycles. Such behavior was likely due the partial decomposition of $Na_3NH_2B_{12}H_{12}$.

One of the most successful demonstration of the Na-ion battery was by employing $Na(B_{12}H_{12})_{0.5}(B_{10}H_{10})_{0.5}$ in a 3 V Na metal cell, which was operated for 250 cycles (Fig. 8 and Table II). This example has represented an important validation on the utility of hydroborates as practical SSEs for relatively high voltage Na ion batteries (Fig. 6) [99]. The key to this successful demonstration was a good contact between the cathode ($NaCrO_2$, theoretical capacity of 120 mA h/g) and the electrolyte, accomplished by impregnating the cathode particles with the electrolyte. This was achieved by dissolving the latter in anhydrous methanol and dispersing $NaCrO_2$ into the solution, followed by drying in a vacuum and heat treatment at 270 °C to recrystallize the electrolyte. This example highlighted the importance of the careful electrode design in enabling hydride-based batteries.

## Electrolytes in rechargeable Mg batteries

Although an electrolyte plays a pivotal role in all battery systems, in the rechargeable magnesium batteries, it is particularly important. Organohalo/organo-based electrolytes are compatible with Mg and perform well; however, they are also corrosive. Lightweight metal hydrides have demonstrated the potential to overcome these problems and based on them a new family of halogen-free salts was reported (see the section titled "Conductivity of lightweight CMHs in Mg batteries"). Due to the high reductive stability of the $[BH_4]^-$ anion, $Mg(BH_4)_2$ is able to withstand the electro/chemical reduction in a reactive environment. This, in turn, prevents the formation of a passivation, nonconductive layer at the magnesium metal anode, which is known to obstruct the battery operation [6, 71, 128, 129]. The performance of the magnesium borohydride-based electrolytes has been tremendously improved by the use of other light-metal hydride complexes: $LiBH_4$ and $NaBH_4$. Although the exact role of these additives is yet to be understood, their presence increases the current density and the efficiency of the plating/stripping processes [6, 71, 128, 129].

The first successful application of non-aqueous $Mg(BH_4)_2$–$LiBH_4$ in DME electrolyte was demonstrated for a battery with a magnesium anode and a Chevrel phase $Mo_6S_8$ cathode [128]. In a following study, the same battery at a rate of C/10 delivered a capacity of 99 mA h/g during the initial discharge (versus 129 mA h/g of the theoretical value) and the reported capacity retention remained at the level of 90% over 300 cycles [71]. Recently, $Mg(BH_4)_2$ in DGM/THFPB was employed in cells with a Mg anode and a Chevrel phase as well as a S/C composite cathode [74]. The $Mo_6S_8$-based battery, operated at various C-rates (0.1–2C), delivered averaged discharge capacities from 72 mA h/g to 21 mA h/g for the lowest and highest C-rates, respectively. At 0.2C, the maintained averaged capacity value was 78–80 mA h/g, over 600 cycles, with the 100% Coulombic efficiency. For the S–C-based battery, the initial discharge capacity reached 956 mA h/g but then dropped to 536 mA h/g after 30 cycles, which accounted for 55% of capacity retention. The most likely reason of the restricted cycling performance was the polysulfide dissolution, which caused the active material loss. The $Mg(BH_4)_2$ in TG as well as $Mg(BH_4)_2$–$LiBH_4$ in TG was also integrated as SSE in a Mg–$Mo_6S_8$ battery, operated at RT and a rate of 0.05C [72]. While the former delivered 66 mA h/g and 63 mA h/g during the initial discharge and charge, respectively, the latter reached 77 and 76 mA h/g during the first discharge–charge cycle. Also, the $LiBH_4$-containing cell revealed stable operation over 107 cycles, with an average discharge of 71 mA h/g and 92% of capacity retention. Lower values were obtained for the same cell with $Mg(BH_4)_2$–$LiBH_4$ in DGM/TG/$PP_{14}$TFSI as SSE [73]. The initial discharge–charge capacity was 74 mA h/g and 57 mA h/g, respectively. The battery

performed in a stable way over next 55 cycles, with the average discharge capacity of 55 mA h/g. The solution of $Mg(BH_4)_2$–$LiBH_4$ applied as an electrolyte in the dual Mg–Li battery with the $FeS_x$ conversion cathode enabled a stable cell operation without dendrite growth [101]. The reversible battery capacity at 0.1C varied between 350 and 400 mA h/g during the first 50 cycles and stayed above 200 mA h/g after the subsequent 150 ones. Interestingly, the solid electrolyte interface formation, containing electrolyte components, was observed at both the cathode and anode. Its presence was likely to suppress the polysulfide dissolution as well as fast passivation of the negative electrode, which resulted in the superior battery performance.

Evaluation of the Mg battery operation was done beyond the $Mg(BH_4)_2$-based liquid electrolytes and included its solid-state derivatives. Highashi et al. applied the synthesized $Mg(BH_4)(NH_2)$ as SSE in the Mg–S, Mg–FeS, and Mg–$Ag_2S$ electrochemical cells, operated at 423 K, however did not report on the charge–discharge performance [69]. Shao et al. implemented the nanocomposite $Mg(BH_4)_2$–PEO–MgO SSE to the Mg SSB and demonstrated its high compatibility with the Chevrel phase as a cathode [100]. The battery showed reversible Mg intercalation/deintercalation and stable operation over 150 cycles at 373 K. The magnesium borohydride-based SSEs may provide higher oxidative stability; however, better understanding of factors that govern their performance in a battery cell is needed.

Studies on the performances of *closo*-borane as electrolytes have also been executed. In particular, the *m*-dicarborane-based Mg salt $Mg(C_2B_{10}H_{12})Cl$ in THF could deliver the expected performance with a Chevrel phase cathode, demonstrating good compatibility [76]. The battery was cycled 30 times at 0.05C and a stable reversible specific capacity of 90 mA h/g was obtained, which corresponded to 90% of the Coulombic efficiency. Magnesium battery was also demonstrated using $Mg(CB_{11}H_{12})_2$ in TG with a Chevrel phase (a follow up work that combined the salt with $Mgphenyl_2$ showed slightly lower performance) [75, 146]. Most importantly, $Mg(CB_{11}H_{11})_2$ in TG was also used to cycle the high voltage cathode α-$MnO_2$, with the initial discharge capacity of 170 mA h/g. This has been the first, successful example of a Mg coin cell operated at voltages exceeding 2.5 V, possible due to overcoming the corrosion problems encountered previously [75].

## Interface stability in lightweight complex metal hydride-based all-SSBs

Given the superior ionic conductivity of the reported light-metal hydride complexes, increase in their σ values is no longer a dominant factor in the development of SSBs. As it has been demonstrated, the focus has shifted toward challenges related to a battery cell integration, which involve the preservation of the electrochemical and mechanical stability of electrodes and

SSEs. Understanding of factors that govern processes at the electrode/SSE interface is crucial for realizing a full potential of lightweight CMHs as SSEs in Li-, Na-, and Mg-based batteries.

Based on the presented examples, it appears that the chemical stability of the electrode/SSE interfaces is of particular importance for the steady SSB operation, as most of the reactions initiate there. While the high reducibility of borohydrides-based SSE provides their good compatibility with Li, Na, and Mg metals, the cathode/SSE contact is critical for the performance of both the SSE and the all-solid-sate battery. Among the identified problems that impede progress in the broad usage of light-metal hydride complexes as SSEs, there is high interfacial resistance, which occurs in a battery mostly due to the detrimental interphase layer formation [77] and/or disruption of the intimate contacts among the electrode, conductive phases, and SSE [78]. Various approaches have been applied to mitigate these undesired effects, as presented in the section titled "LIBs." In the case of the LIB with the $LiCoO_2$ cathode, the reaction observed between oxide and highly reductive $LiBH_4$ SSE caused decomposition of $LiCoO_2$ and deterioration of the cathode/$LiBH_4$ interface, which resulted in capacity loss [77]. In general, formation of inactive by-products at the oxide/borohydride-based SSE contact increases the interfacial resistance, which eventually hinders the transfer of $Li^+$/electrons in the cathode. To suppress this effect, various coating/buffer layers (e.g., $LiNbO_3$ [19], $Li_2PO_4$ [77], $Li_3BO_3$ [80]) have been successfully applied and prevented undesired interactions between the cathode and SSE, which in turn improved the reversibility and durability of the investigated SSBs. The oxide-cathode batteries with borohydride-based SSE often also suffer due to poor electrode/SSE contacts. Thus, the buffer layers (e.g., $LiBH_4 + x LiNH_2$) were also proposed to eliminate surface roughness and to improve the interface compactness [80]. On the other hand, the studied examples also demonstrate that the formation of a stable phase at the electrode/SSE contact does not always carry a negative effect. In the $TiS_2$–Li cell with $LiBH_4$ SSE, the reaction between the cathode material and SSE led to the formation of the interfacial layer of amorphous $Li_2B_{12}H_{12}$, which appeared very beneficial. The high ionic conductivity of $Li_2B_{12}H_{12}$, together with its higher oxidative stability as compared to $LiBH_4$, played a key role in the stable and prolonged battery operation [12, 85].

The reported examples of Na-based SSBs also suggest that the careful design of the battery components is essential for the improved cell operation. The battery with the solution-processed impregnated electrode ($NaCrO_2$–$Na_2(B_{12}H_{12})_{0.5}(B_{10}H_{10})_{0.5}$–super-P) demonstrated the significant reduction of the internal resistance and much better cycling performance, due to a stable intimate contact ensured between the cathode and SSE, which could not be obtained with the same cathode fabricated by simple mixing of composite components [99].

The control of processes at the electrode/SSE interfaces is still very limited, and in-depth theoretical and experimental (operando) studies of their thermodynamics and kinetics are essential to evaluate their fundamental aspects, on the one hand, and to provide practical solutions to current challenges related to SSBs, on the other hand.

## Light-metal hydride complexes as anode active materials in LIBs

Conversion reactions in Li-based batteries can be used as an alternative to intercalation [147]. Their main advantage relies on a multielectron redox process, which could provide much higher specific capacity compared to currently utilized graphite-based anodes. Among various systems proposed as positive and negative materials, hydrides deserve particular consideration. Besides the high theoretical capacities, their electrochemical activity occurs in a safe potential region versus Li [144]. Based on theoretical predictions, for batteries with lightweight CMHs, specific capacities in a range of 2000–4000 mA h/g can be achieved. Thus, the reactivity of selected groups of hydrogen complexes in Li-ion cells has been investigated [94, 95, 96].

### Borohydrides

Meggiolaro et al. reported on the incorporation of the selected borohydrides as active anode materials in a Li-ion cell [94]. The study spanned ball milled $LiBH_4$, $NaBH_4$, $KBH_4$, $Mg(BH_4)_2$, and $Ca(BH_4)_2$, which were tested against Li with a solution of $LiPF_6$ in the ethylene/dimethyl carbonate mixture as an electrolyte. Batteries were evaluated in a potential range of 2.5/2.0–0.01 V and at a rate of C/20. $LiBH_4$, $KBH_4$, and $Ca(BH_4)_2$ showed no or negligible electrochemical activity, which was likely due to limited electron/ionic conductivity of the materials and/or high activation energy of the conversion reaction. More encouraging results were obtained for $NaBH_4$ and $Mg(BH_4)_2$, for which specific capacities reached approximately 200 mA h/g upon the first reduction. The study also emphasized the importance of the relationship between the duration of mechanochemical powder processing and material reactivity. For shorter milled $Mg(BH_4)_2$, a higher number of redox processes in a battery was observed with the first discharge capacity reaching 540 mA h/g. Although the measured capacities were much lower than the theoretical ones, the study showed possible enhancement of the battery performances by the optimization of the active material morphology.

### Alanates

The first demonstration of alanates as conversion anodes in the Li-ion cell was presented for $LiAlH_4$ and $Li_3AlH_6$ by Silvestri et al. [95]. The mechanochemically processed materials were

tested in a three-electrode cell, with Li as a counter electrode and a solution of LiPF$_6$ as an electrolyte, at a rate of C/20, in a potential range of 2.5–0.01 V. The study demonstrated that the reversible incorporation/de-incorporation of Li as well as the occurrence of a conversion reaction in both materials pointed to a high complexity of the reaction mechanism. Even though the capacities upon discharge were as high as 1180 mA h/g and 900 mA h/g for LiAlH$_4$ and Li$_3$AlH$_6$, respectively (versus theoretical values: 2119 mA h/g and 1493 mA h/g), the reversibility of the processes was poor as only 16% and 22% of these values, respectively, were recovered during the subsequent charge cycle. Such behavior was associated with a large volume variation upon conversion (30%) and alloying reactions (100%). In another study, the performance of unprocessed LiAlH$_4$ was tested in the same electrochemical environment at C/10 [148]. The study also confirmed the occurrence of a poorly reversible, conversion reaction between LiAlH$_4$ and Li, with an unclear reaction pathway.

The compatibility of NaAlH$_4$, Na$_3$AlH$_6$, and LiNa$_2$AlH$_6$ with Li electrode in a solution of LiPF$_6$ as an electrolyte was also explored [96, 148]. While the electrochemical performances of both unprocessed and mechanochemically activated compounds were rather poor, the ball milling of NaAlH$_4$ with the conductive carbon showed an impressive increase in the conversion reversibility. This resulted in a much greater value of the charge capacity (1 versus 2.65 lithium equivalents for unprocessed and processed sodium alanate, respectively; theoretical value: 4 lithium equivalents) with almost 70% of Coulombic efficiency [96]. It was suggested that the mechanical powder processing promoted the creation of a highly reactive carbon-hydride composite, which permitted the formation of a solid–electrolyte interface without Li consumption [149]. The composite was also able to mitigate the electrode pulverization upon cycling, which prevented the loss of electronic contact between particles upon discharge–charge cycles. The studies indicated a multistep discharge reaction that proceeded via the formation of intermediate Na$_3$AlH$_6$ and/or LiNa$_2$AlH$_6$ phases; however, the complete mechanism of the NaAlH$_4$ regeneration has not been fully understood. Further improvement in the performance was expected by integration of the nanoconfined sodium alanate in the electrochemical cell. In this case, the reversible conversion reaction in the Li-ion cell with the hydride-based electrode was demonstrated and high values of the initial discharge–charge capacity were reported [97, 98]. However, during the subsequent 20 cycles, the significant loss in the reactivity of nanoconfined NaAlH$_4$ was observed, which caused the substantial fading of the battery reversible capacity.

## Summary and outlook

In this review, we presented an overview of the lightweight CMHs and their composites, with documented ionic conductivity, as well as selected examples of these materials' application in Li-, Na-, and Mg-based batteries.

The discovery of high solid-state ionic conductivity in HT-LiBH$_4$ opened an extensive field of the research on SSEs. This was further stirred by the results showing the successful stabilization of the conductive phase down to RT, by simple halogen anion substitutions. It was found that the enhanced ionic conductivity observed in borhydrides has been due to several factors: disordered distribution of cations and high density of vacancies in the crystal structure of Li- and Na-ion conductors, modification of the structural aperture by the cation/anion substitutions, and high rotational mobility of the [BH$_4$]$^-$ units decreasing activation energy and promoting the Li-ion diffusion. In the case of the hydride-based composites, the additional influence of material phase compositions, microstructural properties, and interfacial processes has been emphasized. The encouraging conductivity results obtained for a new type of compounds such as LiCa$_3$(BH$_4$)(BO$_3$)$_2$ call for investigation of other oxide-hydride compositions that could be important in terms of their high compatibility with the commonly used electrode materials. Also, the recently reported new concept of ammonia gas absorption by LiBH$_4$ is worth exploring in detail to understand the factors of the excellent Li-ion mobility in Li(NH$_3$)BH$_4$ as it could inspire new approaches in designing of superconducting hydride-based materials. The discovery of record Na solid-state conductivities in *closo*-borane compounds represents an important milestone in the consideration of hydrides as SSEs. This area of research was further enriched by implementing concepts similar to those used to improve LiBH$_4$ conductivities as outlined above. In particular, the mixed cluster anion salt systems such as that based on [CB$_9$H$_{10}$CB$_{11}$H$_{12}$]$^{2-}$, which even elevated Li ion conductivities to the levels of most competent Li$^+$ electrolytes, require particular attention. In this case, understanding of key structural factors that govern this performance and establishing the role of thermal treatments on generating these high conductivities are paramount.

In the field of liquid electrolyte research, advancements driven by the discovery of Mg metal compatibility with Mg(BH$_4$)$_2$ electrolytes have disrupted the field of electrolytes for multivalent batteries (Mg, Ca). Research demonstrated the important role BH$_4^-$ plays through its synergy with ether solvent-Mg$^{2+}$ coordination to produce highly performing electroactive species and Mg$^{2+}$ permeable interfaces. These findings motivated investigating borohydride salts as SSEs, which produced the highest conducting Mg electrolyte to date. Highly efficient and practical non-corrosive simple electrolytes were demonstrated with wide electrochemical windows exceeding that of the solvent itself using the *closo*-borane Mg(CB$_{11}$H$_{12}$)$_2$ salt. The scope of hydrides' role in energy storage has been recently expanded beyond the "inorganic salts" form where

organic salts based on *closo*-monocarbone have been reported as highly competent ionic liquid solvents for Mg and Li batteries. Current studies are demonstrating the richness as well as complexity of the hydride salt-solvent and the hydride salt-electrode interactions, so moving forward in-depth studies are needed to determine key bulk and interfacial phenomena at play.

The still limited studies on the application of the LiBH$_4$-based materials as SSEs in Li- and Na-ion batteries have shown their good interfacial contacts with electrodes but also increased capacity and better cyclic stability of batteries using hydride anodes, as compared to their liquid electrolyte-based counterparts. This emphasizes that interfacial effects together with borohydrides' high electrochemical stability and plasticity play an important role in the battery operation. However, further studies are necessary to understand both the nature of involved (electro)chemical processes, on the one hand, and modifications of the battery components in view of the fundament material properties, on the other hand. In the case of rechargeable Mg batteries, Mg(BH$_4$)$_2$ and its derivatives, applied as anhydrous or SSEs, were shown to support the battery function, where, in particular, Mg(CB$_{11}$H$_{12}$)$_2$ in TG solvent enabled unprecedented charging of a Mg coin cell battery to high voltages. However, challenges with the available Mg battery cathodes have limited research of cathode-electrolyte interactions, establishing the true battery performances in such electrolytes. As new working and stable Mg cathodes emerge, it is critical that these electrolytes are studied in a battery setup to identify challenges and opportunities.

## References

1. M. Armand and J.M. Tarascon: Building better batteries. *Nature* **451**, 652 (2008).

2. J.W. Choi and D. Aurbach: Promise and reality of post-lithium-ion batteries with high energy densities. *Nat. Rev. Mater.* **1**, 16013 (2016).

3. R. Mohtadi and F. Mizuno: Magnesium batteries: Current state of the art, issues and future perspectives. *Beilstein J. Nanotechnol.* **5**, 1291 (2014).

4. A. Manthiram, X. Yu, and S. Wang: Lithium battery chemistries enabled by solid-state electrolytes. *Nat. Rev. Mater.* **2**, 16103 (2017).

5. O. Tutusaus and R. Mohtadi: Paving the way towards highly stable and practical electrolytes for rechargeable magnesium batteries. *ChemElectroChem* **2**, 51 (2015).

6. R. Mohtadi and S-I. Orimo: The renaissance of hydrides as energy materials. *Nat. Rev. Mater.* **2**, 16091 (2016).

7. S-I. Orimo, Y. Nakamori, J.R. Eliseo, A. Züttel, and C.M. Jensen: Complex hydrides for hydrogen storage. *Chem. Rev.* **107**, 4111 (2007).

8. M. Paskevicius, L.H. Jepsen, P. Schouwink, R. Cerny, D.B. Ravnsbaek, Y. Filinchuk, M. Dornheim, F. Besenbacherf, and T.R. Jensen: Metal borohydrides and derivatives—Synthesis, structure and properties. *Chem. Soc. Rev.* **46**, 1565 (2017).

9. M. Matsuo, Y. Nakamori, S-I. Orimo, H. Maekawa, and H. Takamura: Lithium superionic conduction in lithium borohydride accompanied by structural transition. *Appl. Phys. Lett.* **91**, 224103 (2007).

10. Y. Nakamori, S-I. Orimo, and T. Tsutaoka: Dehydriding reaction of metal hydrides and alkali borohydrides enhanced by microwave irradiation. *Appl. Phys. Lett.* **88**, 112104 (2006).

11. M. Matsuo and S-I. Orimo: Lithium fast-ionic conduction in complex hydrides: Review and prospects. *Adv. Energy Mater.* **1**, 161 (2011).

12. A. Unemoto, M. Matsuo, and S-I. Orimo: Complex hydrides for electrochemical energy storage. *Adv. Funct. Mater.* **24**, 2267 (2014).

13. D. Sveinbjornsson, J.S.G. Myrdal, D. Blanchard, J.J. Bentzen, T. Hirata, M.B. Mogensen, P. Norby, S-I. Orimo, and T. Vegge: Effect of heat treatment on the lithium ion conduction of the LiBH$_4$–LiI solid solution. *J. Phys. Chem. C* **117**, 3249 (2013).

14. H. Maekawa, M. Matsuo, H. Takamura, M. Ando, Y. Noda, T. Karahashi, and S-I. Orimo: Halide-stabilized LiBH$_4$, a room-temperature lithium fast-ion conductor. *J. Am. Chem. Soc.* **131**, 894 (2009).

15. R. Miyazaki, T. Karahashi, N. Kumatani, Y. Noda, M. Ando, H. Takamura, M. Matsuo, S-I. Orimo, and H. Maekawa: Room temperature lithium fast-ion conduction and phase relationship of LiI stabilized LiBH$_4$. *Solid State Ionics* **192**, 143 (2011).

16. I. Cascallana-Matias, D.A. Keen, E.J. Cussen, and D.H. Gregory: Phase behavior in the LiBH$_4$–LiBr system and structure of the anion-stabilized fast ionic, high temperature phase. *Chem. Mater.* **27**, 7780 (2015).

17. M. Matsuo, H. Takamura, H. Maekawa, H.W. Li, and S-I. Orimo: Stabilization of lithium superionic conduction phase and enhancement of conductivity of LiBH$_4$ by LiCl addition. *Appl. Phys. Lett.* **94**, 084103 (2009).

18. H. Oguchi, M. Matsuo, T. Sato, H. Takamura, H. Maekawa, H. Kuwano, and S-I. Orimo: Lithium-ion conduction in complex hydrides LiAlH$_4$ and Li$_3$AlH$_6$. *J. Appl. Phys.* **107**, 096104 (2010).

19. A. Unemoto, G. Nogami, M. Tazawa, M. Taniguchi, and S-I. Orimo: Development of 4V-class bulk-type all-solid-state lithium rechargeable batteries by a combined use of complex hydride and sulfide electrolytes for room temperature operation. *Mater. Trans., JIM* **58**, 1063 (2017).

20. M. Matsuo, A. Remhof, P. Martelli, R. Caputo, M. Ernst, Y. Miura, T. Sato, H. Oguchi, H. Maekawa, H. Takamura, A. Borgschulte, A. Zuttel, and S-I. Orimo: Complex hydrides

with $(BH_4)^-$ and $(NH_2)^-$ anions as new lithium fast-ion conductors. *J. Am. Chem. Soc.* **131**, 16389 (2009).

21. W. Li, G.T. Wu, Z.T. Xiong, Y.P. Feng, and P. Chen: $Li^+$ ionic conductivities and diffusion mechanisms in Li-based imides and lithium amide. *Phys. Chem. Chem. Phys.* **14**, 1596 (2012).

22. Y. Yan, R-S. Kühnel, A. Remhof, L. Duchêne, E.C. Reyes, D. Rentsch, Z. Łodziana, and C. Battaglia: A lithium amide-borohydride solid-state electrolyte with lithium-ion conductivities comparable to liquid electrolytes. *Adv. Energy Mater.* **7**, 1700294 (2017).

23. A. Wolczyk, B. Paik, T. Sato, C. Nervi, M. Brighi, S.P. GharibDoust, M. Chierotti, M. Matsuo, G.Q. Li, R. Gobetto, T.R. Jensen, R. Cerny, S-I. Orimo, and M. Baricco: $Li_5(BH_4)_3NH$: Lithium-rich mixed anion complex hydride. *J. Phys. Chem. C* **121**, 11069 (2017).

24. E. Roedern, Y.S. Lee, M.B. Ley, K. Park, Y.W. Cho, J. Skibsted, and T.R. Jensen: Solid state synthesis, structural characterization and ionic conductivity of bimetallic alkali-metal yttrium borohydrides $MY(BH_4)_4$ (M = Li and Na). *J. Mater. Chem. A* **4**, 8793 (2016).

25. M.B. Ley, D.B. Ravnsbæk, Y. Filinchuk, Y-S. Lee, R. Janot, Y.W. Cho, J. Skibsted, and T.R. Jensen: $LiCe(BH_4)_3Cl$, a new lithium-ion conductor and hydrogen storage material with isolated tetranuclear anionic clusters. *Chem. Mater.* **24**, 1654 (2012).

26. Y-S. Lee, M.B. Ley, T.R. Jensen, and Y.W. Cho: Lithium ion disorder and conduction mechanism in $LiCe(BH_4)_3Cl$. *J. Phys. Chem. C* **120**, 19035 (2016).

27. S.P. GharibDoust, M. Brighi, Y. Sadikin, D.B. Ravnsbaek, R. Cerny, J. Skibsted, and T.R. Jensen: Synthesis, structure, and Li-ion conductivity of $LiLa(BH_4)_3X$, X = Cl, Br, I. *J. Phys. Chem. C* **121**, 19010 (2017).

28. R. Cerny, P. Schouwink, Y. Sadikin, K. Stare, L. Smrcok, B. Richter, and T.R. Jensen: Trimetallic borohydride $Li_3MZn_5(BH_4)_{15}$ (M = Mg, Mn) containing two weakly interconnected frameworks. *Inorg. Chem.* **52**, 9941 (2013).

29. Y. Sadikin, K. Stare, P. Schouwink, M.B. Ley, T.R. Jensen, A. Meden, and R. Cerny: Alkali metal—yttrium borohydrides: The link between coordination of small and large rare-earth. *J. Solid State Chem.* **225**, 231 (2015).

30. M. Brighi, P. Schouwink, Y. Sadikin, and R. Cerny: Fast ion conduction in garnet-type metal borohydrides $Li_3K_3Ce_2(BH_4)_{12}$ and $Li_3K_3La_2(BH_4)_{12}$. *J. Alloys Compd.* **662**, 388 (2016).

31. E. Didelot and R. Cerny: Ionic conduction in bimetallic borohydride borate, $LiCa_3(BH_4)(BO_3)_2$. *Solid State Ionics* **305**, 16 (2017).

32. T. Zhang, Y. Wang, T. Song, H. Miyaoka, K. Shinzato, H. Miyaoka, T. Ichikawa, S. Shi, X. Zhang, S. Isobe, N. Hashimoto, and Y. Kojima: Ammonia, a switch for controlling high ionic conductivity in lithium borohydride ammoniates. *Joule* **2**, 1522 (2018).

33. D. Blanchard, A. Nale, D. Sveinbjornsson, T.M. Eggenhuisen, M.H.W. Verkuijlen, Suwarno, T. Vegge, A.P.M. Kentgens, and P.E. de Jongh: Nanoconfined $LiBH_4$ as a fast lithium ion conductor. *Adv. Funct. Mater.* **25**, 184 (2015).

34. Y.S. Choi, Y.S. Lee, K.H. Oh, and Y.W. Cho: Interface-enhanced Li ion conduction in a $LiBH_4$–$SiO_2$ solid electrolyte. *Phys. Chem. Chem. Phys.* **18**, 22540 (2016).

35. Y.S. Choi, Y.S. Lee, D.J. Choi, K.H. Chae, K.H. Oh, and Y.W. Cho: Enhanced Li ion conductivity in $LiBH_4$–$Al_2O_3$ mixture via interface engineering. *J. Phys. Chem. C* **121**, 26209 (2017).

36. J.A. Teprovich, H.R. Colon-Mercado, P.A. Ward, B. Peters, S. Giri, J. Zhou, S. Greenway, R.N. Compton, P. Jena, and R. Zidan: Experimental and theoretical analysis of fast lithium ionic conduction in a $LiBH_4$–$C_{60}$ nanocomposite. *J. Phys. Chem. C* **118**, 21755 (2014).

37. L. Zhan, Y. Zhang, X. Zhuang, H. Fang, Y. Zhu, X. Guo, J. Chen, Z. Wang, and L. Li: Ionic conductivities of lithium borohydride–lithium nitride composites. *Solid State Ionics* **304**, 150 (2017).

38. Y. Zhang, L.Y. Zhan, X.Y. Zhuang, Y.F. Zhu, N. Wan, X.L. Guo, J. Chen, Z.M. Wang, and L.Q. Li: The ionic conductivities, stabilities and ionic mobilities of $xLiBH_4$–$Li_2NH$ (x = 1, 2, 4) composites as fast ion conductor. *J. Alloys Compd.* **695**, 2894 (2017).

39. H. Wang, H.J. Cao, W.J. Zhang, J. Chen, H. Wu, C. Pistidda, X.H. Ju, W. Zhou, G.T. Wu, M. Etter, T. Klassen, M. Dornheim, and P. Chen: $Li_2NH$–$LiBH_4$: A complex hydride with near ambient hydrogen adsorption and fast lithium ion conduction. *Chem. - Eur. J.* **24**, 1342 (2018).

40. D. Sveinbjörnsson, D. Blanchard, J.S.G. Myrdal, R. Younesi, R. Viskinde, M.D. Riktor, P. Norby, and T. Vegge: Ionic conductivity and the formation of cubic $CaH_2$ in the $LiBH_4$–$Ca(BH_4)_2$ composite. *J. Solid State Chem.* **211**, 81 (2014).

41. M. Xiang, Y. Zhang, L. Zhan, Y. Zhu, X. Guo, J. Chen, Z. Wang, and L. Li: Study on $xLiBH_4$–$NaBH_4$ (x = 1.6, 2.3, and 4) composites with enhanced lithium ionic conductivity. *J. Alloys Compd.* **729**, 936 (2017).

42. P. López-Aranguren, N. Berti, A.H. Dao, J. Zhang, F. Cuevas, M. Latroche, and C. Jordy: An all-solid-state metal hydride—Sulfur lithium-ion battery. *J. Power Sources* **357**, 56 (2017).

43. M. Xiang, Y. Zhang, Y. Zhu, X. Guo, J. Chen, and L. Li: Ternary $LiBH_4$–$NaBH_4$–$MgH_2$ composite as fast ionic conductor. *Solid State Ionics* **324**, 109 (2018).

44. M. Xiang, Y. Zhang, H. Lin, Y. Zhu, X. Guo, J. Chen, and L. Li: $LiBH_4$–NaX (X = Cl, I) composites with enhanced lithium ionic conductivity. *J. Alloys Compd.* **764**, 307 (2018).

45. A. Unemoto, H. Wu, T.J. Udovic, M. Matsuo, T. Ikeshoji, and S-I. Orimo: Fast lithium-ionic conduction in a new complex hydride–sulphide crystalline phase. *Chem. Commun.* **52**, 564 (2016).

46. A. Yamauchi, A. Sakuda, A. Hayashi, and M. Tatsumisago: Preparation and ionic conductivities of $(100 - x)(0.75Li_2S \cdot 0.25P_2S_5) \cdot xLiBH_4$ glass electrolytes. *J. Power Sources* **244**, 707 (2013).

47. A. El Kharbachi, Y. Hu, K. Yoshida, P. Vajeeston, S. Kim, M.H. Sorby, S-I. Orimo, H. Fjellvag, and B.C. Hauback: Lithium ionic conduction in composites of $Li(BH_4)_{0.75}I_{0.25}$ and amorphous $0.75Li_2S \cdot 0.25P_2S_5$ for battery applications. *Electrochim. Acta* **278**, 332 (2018).

48. B.A. Boukamp and R.A. Huggins: Ionic conductivity in lithium imide. *Phys. Lett. A* **72**, 464 (1979).

49. J. Rijssenbeek, Y. Gao, J. Hanson, Q. Huang, C. Jones, and B. Toby: Crystal structure determination and reaction pathway of amide-hydride mixtures. *J. Alloys Compd.* **454**, 233 (2008).

50. W.S. Tang, M. Matsuo, H. Wu, V. Stavila, A. Unemoto, S-I. Orimo, and T.J. Udovic: Stabilizing lithium and sodium fast-ion conduction in solid polyhedral-borate salts at device-relevant temperatures. *Energy Storage Mater.* **4**, 79 (2016).

51. J.A. Teprovich, H. Colon-Mercado, A.L. Washington, Ii, P.A. Ward, S. Greenway, D.M. Missimer, H. Hartman, J. Velten, J.H. Christian, and R. Zidan: Bi-functional $Li_2B_{12}H_{12}$ for energy storage and conversion applications: Solid-state electrolyte and luminescent down-conversion dye. *J. Mater. Chem. A* **3**, 22853 (2015).

52. S. Kim, N. Toyama, H. Oguchi, T. Sato, S. Takagi, T. Ikeshoji, and S-I. Orimo: Fast lithium-ion conduction in atom-deficient *closo*-type complex hydride solid electrolytes. *Chem. Mater.* **30**, 386 (2018).

53. Y. Yan, D. Rentsch, C. Battaglia, and A. Remhof: Synthesis, stability and Li-ion mobility of nanoconfined $Li_2B_{12}H_{12}$. *Dalton Trans.* **46**, 12434 (2017).

54. L. He, H-W. Li, H. Nakajima, N. Tumanov, Y. Filinchuk, S-J. Hwang, M. Sharma, H. Hagemann, and E. Akiba: Synthesis of a bimetallic dodecaborate $LiNaB_{12}H_{12}$ with otstanding suerionic cnductivity. *Chem. Mater.* **27**, 5483 (2015).

55. W.S. Tang, A. Unemoto, W. Zhou, V. Stavila, M. Matsuo, H. Wu, S-I. Orimo, and T.J. Udovic: Unparalleled lithium and sodium superionic conduction in solid electrolytes with large monovalent cage-like anions. *Energy Environ. Sci.* **8**, 3637 (2015).

56. W. Tang, M. Matsuo, H. Wu, V. Stavila, W. Zhou, A. Talin, A.V. Soloninin, R.V. Skoryunov, O.A. Babanova, A.V. Skripov, A. Unemoto, S-I. Orimo, and T.J. Udovic: Liquid-like ionic conduction in solid lithium and sodium monocarba-*closo*-decaborates near or at room temperature. *Adv. Energy Mater.* **6**, 1502237 (2016).

57. W.S. Tang, K. Yoshida, A.V. Soloninin, R.V. Skoryunov, O.A. Babanova, A.V. Skripov, M. Dimitrievska, V. Stavila, S-I. Orimo, and T.J. Udovic: Stabilizing superionic-conducting structures via mixed-anion solid solutions of monocarba-*closo*-borate salts. *ACS Energy Lett.* **1**, 659 (2016).

58. M. Matsuo, S. Kuromoto, T. Sato, H. Oguchi, H. Takamura, and S-I. Orimo: Sodium ionic conduction in complex hydrides with $[BH_4]^-$ and $[NH_2]^-$ anions. *Appl. Phys. Lett.* **100**, 203904 (2012).

59. M. Matsuo, H. Oguchi, T. Sato, H. Takamura, E. Tsuchida, T. Ikeshoji, and S-I. Orimo: Sodium and magnesium ionic conduction in complex hydrides. *J. Alloys Compd.* **580**, S98 (2013).

60. Y. Sadikin, M. Brighi, P. Schouwink, and R. Cerny: Superionic conduction of sodium and lithium in anion-mixed hydroborates $Na_3BH_4B_{12}H_{12}$ and $(Li_{0.7}Na_{0.3})_3BH_4B_{12}H_{12}$. *Adv. Energy Mater.* **5**, 1501016 (2015).

61. L. He, H. Lin, H-F. Li, Y. Filinchuk, J. Zhang, Y. Liu, M. Yang, Y. Hou, Y. Deng, H-W. Li, H. Shao, L. Wang, and Z. Lu: $Na_3NH_2B_{12}H_{12}$ as high performance solid electrolyte for all-solid-state Na-ion batteries. *J. Power Sources* **396**, 574 (2018).

62. H. Oguchi, M. Matsuo, S. Kuronnoto, H. Kuwano, and S-I. Orimo: Sodium-ion conduction in complex hydrides $NaAlH_4$ and $Na_3AlH_6$. *J. Appl. Phys.* **111**, 036102 (2012).

63. T.J. Udovic, M. Matsuo, A. Unemoto, N. Verdal, V. Stavila, A.V. Skripov, J.J. Rush, H. Takamura, and S-I. Orimo: Sodium superionic conduction in $Na_2B_{12}H_{12}$. *Chem. Commun.* **50**, 3750 (2014).

64. B.R.S. Hansen, M. Paskevicius, M. Jørgensen, and T.R. Jensen: Halogenated sodium-*closo*-dodecaboranes as solid-state ion conductors. *Chem. Mater.* **29**, 3423 (2017).

65. T.J. Udovic, M. Matsuo, W.S. Tang, H. Wu, V. Stavila, A.V. Soloninin, R.V. Skoryunov, O.A. Babanova, A.V. Skripov, J.J. Rush, A. Unemoto, H. Takamura, and S-I. Orimo: Exceptional superionic conductivity in disordered sodium decahydro-*closo*-decaborate. *Adv. Mater.* **26**, 7622 (2014).

66. L. Duchene, R.S. Kuhnel, D. Rentsch, A. Remhof, H. Hagemann, and C. Battaglia: A highly stable sodium solid-state electrolyte based on a dodeca/deca-borate equimolar mixture. *Chem. Commun.* **53**, 4195 (2017).

67. K. Yoshida, T. Sato, A. Unemoto, M. Matsuo, T. Ikeshoji, T.J. Udovic, and S-I. Orimo: Fast sodium ionic conduction in $Na_2B_{10}H_{10}$–$Na_2B_{12}H_{12}$ pseudo-binary complex hydride and application to a bulk-type all-solid-state battery. *Appl. Phys. Lett.* **110**, 103901 (2017).

68. W.S. Tang, M. Dimitrievska, V. Stavila, W. Zhou, H. Wu, A.A. Talin, and T.J. Udovic: Order–disorder transitions and superionic conductivity in the sodium *nido*-undeca(carba) borates. *Chem. Mater.* **29**, 10496 (2017).

69. S. Higashi, K. Miwa, M. Aoki, and K. Takechi: A novel inorganic solid state ion conductor for rechargeable Mg batteries. *Chem. Commun.* **50**, 1320 (2014).

70. E. Roedern, R-S. Kühnel, A. Remhof, and C. Battaglia: Magnesium ethylenediamine borohydride as solid-state electrolyte for magnesium batteries. *Sci. Rep.* **7**, 46189 (2017).

71. **Y. Shao, T. Liu, G. Li, M. Gu, Z. Nie, M. Engelhard, J. Xiao, D. Lv, C. Wang, J-G. Zhang, and J. Liu**: Coordination chemistry in magnesium battery electrolytes: How ligands affect their performance. *Sci. Rep.* **3**, 3130 (2013).

72. **F. Tuerxun, Y. Abulizi, Y.N. NuLi, S.J. Su, J. Yang, and J.L. Wang**: High concentration magnesium borohydride/tetraglyme electrolyte for rechargeable magnesium batteries. *J. Power Sources* **276**, 255 (2015).

73. **S.J. Su, Y. Nuli, N. Wang, D. Yusipu, J. Yang, and J.L. Wang**: Magnesium borohydride-based electrolytes containing 1-butyl-1-methylpiperidinium bis(trifluoromethyl sulfonyl)imide ionic liquid for rechargeable magnesium batteries. *J. Electrochem. Soc.* **163**, D682 (2016).

74. **H.M. Xu, Z.H. Zhang, J.J. Li, L.X. Qiao, C.L. Lu, K. Tang, S.M. Dong, J. Ma, Y.J. Liu, X.H. Zhou, and G.L. Cui**: Multifunctional additives improve the electrolyte properties of magnesium borohydride toward magnesium–sulfur batteries. *ACS Appl. Mater. Interfaces* **10**, 23757 (2018).

75. **O. Tutusaus, R. Mohtadi, T.S. Arthur, F. Mizuno, E.G. Nelson, and Y.V. Sevryugina**: An efficient halogen-free electrolyte for use in rechargeable magnesium batteries. *Angew. Chem., Int. Ed.* **54**, 7900 (2015).

76. **T.J. Carter, R. Mohtadi, T.S. Arthur, F. Mizuno, R. Zhang, S. Shirai, and J.W. Kampf**: Boron clusters as highly stable magnesium-battery electrolytes. *Angew. Chem., Int. Ed.* **126**, 3237 (2014).

77. **K. Takahashi, K. Hattori, T. Yamazaki, K. Takada, M. Matsuo, S-I. Orimo, H. Maekawa, and H. Takamura**: All-solid-state lithium battery with LiBH$_4$ solid electrolyte. *J. Power Sources* **226**, 61 (2013).

78. **D. Sveinbjörnsson, A.S. Christiansen, R. Viskinde, P. Norby, and T. Vegge**: The LiBH$_4$–LiI solid solution as an electrolyte in an all-solid-state battery. *J. Electrochem. Soc.* **161**, A1432 (2014).

79. **K. Yoshida, S. Suzuki, J. Kawaji, A. Unemoto, and S-I. Orimo**: Complex hydride for composite negative electrode—Applicable to bulk-type all-solid-state Li-ion battery with wide temperature operation. *Solid State Ionics* **285**, 96 (2016).

80. **S. Suzuki, J. Kawaji, K. Yoshida, A. Unemoto, and S-I. Orimo**: Development of complex hydride-based all-solid-state lithium ion battery applying low melting point electrolyte. *J. Power Sources* **359**, 97 (2017).

81. **A. Unemoto, S. Yasaku, G. Nogami, M. Tazawa, M. Taniguchi, M. Matsuo, T. Ikeshoji, and S-I. Orimo**: Development of bulk-type all-solid-state lithium-sulfur battery using LiBH$_4$ electrolyte. *Appl. Phys. Lett.* **105**, 083901 (2014).

82. **A. Unemoto, C. Chen, Z. Wang, M. Matsuo, T. Ikeshoji, and S-I. Orimo**: Pseudo-binary electrolyte, LiBH$_4$–LiCl, for bulk-type all-solid-state lithium–sulfur battery. *Nanotechnology* **26**, 254001 (2015).

83. **S. Das, P. Ngene, P. Norby, T. Vegge, P.E. de Jongh, and D. Blanchard**: All-solid-state lithium–sulfur battery based on a nanoconfined LiBH$_4$ electrolyte. *J. Electrochem. Soc.* **163**, A2029 (2016).

84. **J. Nguyen, B. Fleutot, and R. Janot**: Investigation of the stability of metal borohydrides-based compounds LiM(BH$_4$)$_3$Cl (M = La, Ce, Gd) as solid electrolytes for Li–S batteries. *Solid State Ionics* **315**, 26 (2018).

85. **A. Unemoto, T. Ikeshoji, S. Yasaku, M. Matsuo, V. Stavila, T.J. Udovic, and S-I. Orimo**: Stable interface formation between TiS$_2$ and LiBH$_4$ in bulk-type all-solid-state lithium batteries. *Chem. Mater.* **27**, 5407 (2015).

86. **A. El Kharbachi, Y. Hu, M.H. Sorby, J.P. Maehlen, P.E. Vullum, H. Fjellvag, and B.C. Hauback**: Reversibility of metal-hydride anodes in all-solid-state lithium secondary battery operating at room temperature. *Solid State Ionics* **317**, 263 (2018).

87. **L. Zeng, K. Kawahito, S. Ikeda, T. Ichikawa, H. Miyaoka, and Y. Kojima**: Metal hydride-based materials towards high performance negative electrodes for all-solid-state lithium-ion batteries. *Chem. Commun.* **51**, 9773 (2015).

88. **L. Zeng, K. Kawahito, and T. Ichikawa**: *Metal Hydride-Based Materials as Negative Electrode for All-Solid-State Lithium-Ion Batteries* (IntechOpen, London, U.K., 2016).

89. **L. Zeng, T. Ichikawa, K. Kawahito, H. Miyaoka, and Y. Kojima**: Bulk-type all-solid-state lithium-ion batteries: Remarkable performances of a carbon nanofiber-supported MgH$_2$ composite electrode. *ACS Appl. Mater. Interfaces* **9**, 2261 (2017).

90. **A. El Kharbachi, H. Uesato, H. Kawai, S. Wenner, H. Miyaoka, M.H. Sørby, H. Fjellvåg, T. Ichikawa, and B.C. Hauback**: MgH$_2$–CoO: A conversion-type composite electrode for LiBH$_4$-based all-solid-state lithium ion batteries. *RSC Adv.* **8**, 23468 (2018).

91. **P. Huen and D.B. Ravnsbæk**: All-solid-state lithium batteries—The Mg$_2$FeH$_6$-electrode LiBH$_4$-electrolyte system. *Electrochem. Commun.* **87**, 81 (2018).

92. **A.J. Weeks, C.S. Tinkey, A.P. Ward, R. Lascola, R. Zidan, and A.J. Teprovich**: Investigation of the reversible lithiation of an oxide free aluminum anode by a LiBH$_4$ solid state electrolyte. *Inorganics* **5**, 1 (2017).

93. **R. Singh, P. Kumari, R.K. Rathore, K. Shinzato, T. Ichikawa, A.S. Verma, V.K. Saraswat, K. Awasthi, A. Jain, and M. Kumar**: LiBH$_4$ as solid electrolyte for Li-ion batteries with Bi$_2$Te$_3$ nanostructured anode. *Int. J. Hydrogen Energy* **43**, 21709 (2018).

94. **D. Meggiolaro, L. Farina, L. Silvestri, S. Panero, S. Brutti, and P. Reale**: Lightweight borohydrides electro-activity in lithium cells. *Energies* **9**, 238 (2016).

95. **L. Silvestri, S. Forgia, L. Farina, D. Meggiolaro, S. Panero, A. La Barbera, S. Brutti, and P. Reale**: Lithium alanates as negative electrodes in lithium-ion batteries. *ChemElectroChem* **2**, 877 (2015).

96. **L. Silvestri, L. Farina, D. Meggiolaro, S. Panero, F. Padella, S. Brutti, and P. Reale**: Reactivity of sodium alanates in lithium batteries. *J. Phys. Chem. C* **119**, 28766 (2015).

97. L. Silvestri, A. Paolone, L. Cirrincione, P. Stallworth, S. Greenbaum, S. Panero, S. Brutti, and P. Reale: NaAlH$_4$ nanoconfinement in a mesoporous carbon for application in lithium ion batteries. *J. Electrochem. Soc.* **164**, A1120 (2017).

98. P. Huen, F. Peru, G. Charalambopoulou, T.A. Steriotis, T.R. Jensen, and D.B. Ravnsbæk: Nanoconfined NaAlH$_4$ conversion electrodes for Li batteries. *ACS Omega* **2**, 1956 (2017).

99. L. Duchene, R.S. Kuhnel, E. Stilp, E. Cuervo Reyes, A. Remhof, H. Hagemann, and C. Battaglia: A stable 3 V all-solid-state sodium-ion battery based on a closo-borate electrolyte. *Energy Environ. Sci.* **10**, 2609 (2017).

100. Y.Y. Shao, N.N. Rajput, J.Z. Hu, M. Hu, T.B. Liu, Z.H. Wei, M. Gu, X.C. Deng, S.C. Xu, K.S. Han, J.L. Wang, Z.M. Nie, G.S. Li, K.R. Zavadil, J. Xiao, C.M. Wang, W.A. Henderson, J.G. Zhang, Y. Wang, K.T. Mueller, K. Persson, and J. Liu: Nanocomposite polymer electrolyte for rechargeable magnesium batteries. *Nano Energy* **12**, 750 (2015).

101. Y. Zhang, J. Xie, Y. Han, and C. Li: Dual-salt Mg-based batteries with conversion cathodes. *Adv. Funct. Mater.* **25**, 7300 (2015).

102. T. Ikeshoji, E. Tsuchida, S. Takagi, M. Matsuo, and S-I. Orimo: Magnesium ion dynamics in Mg(BH$_4$)$_{2(1-x)}$X$_{2x}$ (X = Cl or AlH$_4$) from first-principles molecular dynamics simulations. *RSC Adv.* **4**, 1366 (2014).

103. K. Miwa, N. Ohba, S. Towata, Y. Nakamori, and S-I. Orimo: First-principles study on lithium borohydride LiBH$_4$. *Phys. Rev. B: Condens. Matter* **69**, 245120 (2004).

104. E. Orgaz, A. Membrillo, R. Castaneda, and A. Aburto: Electronic structure of ternary hydrides based on light elements. *J. Alloys Compd.* **404**, 176 (2005).

105. F. Buchter, Z. Lodziana, P. Mauron, A. Remhof, O. Friedrichs, A. Borgschulte, A. Zuttel, D. Sheptyakov, T. Strassle, and A.J. Ramirez-Cuesta: Dynamical properties and temperature induced molecular disordering of LiBH$_4$ and LiBD$_4$. *Phys. Rev. B: Condens. Matter* **78**, 094302 (2008).

106. A. Remhof, Z. Lodziana, P. Martelli, O. Friedrichs, A. Zuttel, A.V. Skripov, J.P. Embs, and T. Strassle: Rotational motion of BH$_4$ units in MBH$_4$ (M = Li, Na, K) from quasielastic neutron scattering and density functional calculations. *Phys. Rev. B: Condens. Matter* **81**, 214304 (2010).

107. C.C. Stephenson, D.W. Rice, and W.H. Stockmayer: Order-disorder transitions in the alkali borohydrides. *J. Chem. Phys.* **23**, 1960 (1955).

108. H. Oguchi, M. Matsuo, J.S. Hummelshoj, T. Vegge, J.K. Norskov, T. Sato, Y. Miura, H. Takamura, H. Maekawa, and S-I. Orimo: Experimental and computational studies on structural transitions in the LiBH$_4$–LiI pseudobinary system. *Appl. Phys. Lett.* **94**, 141912 (2009).

109. A.V. Skripov, A.V. Soloninin, L.H. Rude, T.R. Jensen, and Y. Filinchuk: Nuclear magnetic resonance studies of reorientational motion and Li diffusion in LiBH$_4$–LiI solid solutions. *J. Phys. Chem. C* **116**, 26177 (2012).

110. V. Epp and M. Wilkening: Fast Li diffusion in crystalline LiBH$_4$ due to reduced dimensionality: Frequency-dependent NMR spectroscopy. *Phys. Rev. B: Condens. Matter* **82**, 020301 (2010).

111. Y. Filinchuk, D. Chernyshov, and R. Cerny: Lightest borohydride probed by synchrotron X-ray diffraction: Experiment calls for a new theoretical revision. *J. Phys. Chem. C* **112**, 10579 (2008).

112. A. Bunde, W. Dieterich, and E. Roman: Dispersed ionic conductors and percolation theory. *Phys. Rev. Lett.* **55**, 5 (1985).

113. Y.S. Lee, Y. Filinchuk, H.S. Lee, J.Y. Suh, J.W. Kim, J.S. Yu, and Y.W. Cho: On the formation and the structure of the first bimetallic borohydride borate, LiCa$_3$(BH$_4$)(BO$_3$)$_2$. *J. Phys. Chem. C* **115**, 10298 (2011).

114. P. Martelli, A. Remhof, A. Borgschulte, R. Ackermann, T. Strassle, J.P. Embs, M. Ernst, M. Matsuo, S-I. Orimo, and A. Zuttel: Rotational motion in LiBH$_4$/LiI solid solutions. *J. Phys. Chem. A* **115**, 5329 (2011).

115. A.V. Skripov, A.V. Soloninin, M.B. Ley, T.R. Jensen, and Y. Filinchuk: Nuclear magnetic resonance studies of BH$_4$ reorientations and Li diffusion in LiLa(BH$_4$)$_3$Cl. *J. Phys. Chem. C* **117**, 14965 (2013).

116. M. Jansen: Volume effect or paddle-wheel mechanism—Fast alkali-metal ionic-conduction in solids with rotationally disordered complex anions. *Angew. Chem., Int. Ed.* **30**, 1547 (1991).

117. P. Schouwink, M.B. Ley, A. Tissot, H. Hagemann, T.R. Jensen, L. Smrcok, and R. Cerny: Structure and properties of complex hydride perovskite materials. *Nat. Commun.* **5**, 5706 (2014).

118. R. Mohtadi: High Li-ion conductivity in a hydride-type solid-state electrolyte: The ammonia effect. *Chem* **4**, 1770 (2018).

119. P. Ngene, P. Adelhelm, A.M. Beale, K.P. de Jong, and P.E. de Jongh: LiBH$_4$/SBA-15 nanocomposites prepared by melt infiltration under hydrogen pressure: Synthesis and hydrogen sorption properties. *J. Phys. Chem. C* **114**, 6163 (2010).

120. N. Verdal, T.J. Udovic, J.J. Rush, X.F. Liu, E.H. Majzoub, J.J. Vajo, and A.F. Gross: Dynamical perturbations of tetrahydroborate anions in LiBH$_4$ due to nanoconfinement in controlled-pore carbon scaffolds. *J. Phys. Chem. C* **117**, 17983 (2013).

121. W. Li, G. Wu, C.M. Araújo, R.H. Scheicher, A. Blomqvist, R. Ahuja, Z. Xiong, Y. Feng, and P. Chen: Li$^+$ ion conductivity and diffusion mechanism in α-Li$_3$N and β-Li$_3$N. *Energy Environ. Sci.* **3**, 1524 (2010).

122. G.T. Wu, Z.T. Xiong, T. Liu, Y.F. Liu, J.J. Hu, P. Chen, Y.P. Feng, and A.T.S. Wee: Synthesis and characterization of a new ternary imide-Li$_2$Ca(NH)$_2$. *Inorg. Chem.* **46**, 517 (2007).

123. C. Vaalma, D. Buchholz, M. Weil, and S. Passerini: A cost and resource analysis of sodium-ion batteries. *Nat. Rev. Mater.* **3**, 18013 (2018).

124. **M. Somer, S. Acar, C. Koz, I. Kokal, P. Hohn, R. Cardoso-Gil, U. Aydemir, and L. Akselrud**: α- and β-Na$_2$[BH$_4$][NH$_2$]: Two modifications of a complex hydride in the system NaNH$_2$–NaBH$_4$; syntheses, crystal structures, thermal analyses, mass and vibrational spectra. *J. Alloys Compd.* **491**, 98 (2010).

125. **A. Hooper**: Study of electrical properties of single crystal and polycrystalline β-alumina using complex plane analysis. *J. Phys. D: Appl. Phys.* **10**, 1487 (1977).

126. **O. Bohnke, S. Ronchetti, and D. Mazza**: Conductivity measurements on nasicon and nasicon-modified materials. *Solid State Ionics* **122**, 127 (1999).

127. **A. Hayashi, K. Noi, A. Sakuda, and M. Tatsumisago**: Superionic glass-ceramic electrolytes for room-temperature rechargeable sodium batteries. *Nat. Commun.* **3**, 856 (2012).

128. **R. Mohtadi, M. Matsui, T.S. Arthur, and S.J. Hwang**: Magnesium borohydride: From hydrogen storage to magnesium battery. *Angew. Chem., Int. Ed. Engl.* **51**, 9780 (2012).

129. **R. Mohtadi, A. Remhof, and P. Jena**: Complex metal borohydrides: Multifunctional materials for energy storage and conversion. *J. Phys.: Condens. Matter* **28**, 353001 (2016).

130. **N. Amir, Y. Vestfrid, O. Chusid, Y. Gofer, and D. Aurbach**: Progress in nonaqueous magnesium electrochemistry. *J. Power Sources* **174**, 1234 (2007).

131. **D. Aurbach, Z. Lu, A. Schechter, Y. Gofer, H. Gizbar, R. Turgeman, Y. Cohen, M. Moshkovich, and E. Levi**: Prototype systems for rechargeable magnesium batteries. *Nature* **407**, 724 (2000).

132. **H.D. Yoo, I. Shterenberg, Y. Gofer, G. Gershinsky, N. Pour, and D. Aurbach**: Mg rechargeable batteries: An on-going challenge. *Energy Environ. Sci.* **6**, 2265 (2013).

133. **M. Matsui**: Study on electrochemically deposited Mg metal. *J. Power Sources* **196**, 7048 (2011).

134. **D. Aurbach, Y. Cohen, and M. Moshkovich**: The study of reversible magnesium deposition by in situ scanning tunneling microscopy. *Electrochem. Solid-State Lett.* **4**, A113 (2001).

135. **J. Muldoon, C.B. Bucur, A.G. Oliver, T. Sugimoto, M. Matsui, H.S. Kim, G.D. Allred, J. Zajicek, and Y. Kotani**: Electrolyte roadblocks to a magnesium rechargeable battery. *Energy Environ. Sci.* **5**, 5941 (2012).

136. **D. Wang, X. Gao, Y. Chen, L. Jin, C. Kuss, and P.G. Bruce**: Plating and stripping calcium in an organic electrolyte. *Nat. Mater.* **17**, 16 (2017).

137. **M. Paskevicius, M.P. Pitt, D.H. Brown, D.A. Sheppard, S. Chumphongphan, and C.E. Buckley**: First-order phase transition in the Li$_2$B$_{12}$H$_{12}$ system. *Phys. Chem. Chem. Phys.* **15**, 15825 (2013).

138. **A.V. Skripov, O.A. Babanova, A.V. Soloninin, V. Stavila, N. Verdal, T.J. Udovic, and J.J. Rush**: Nuclear magnetic resonance study of atomic motion in A$_2$B$_{12}$H$_{12}$ (A = Na, K, Rb, Cs): Anion reorientations and Na$^+$ mobility. *J. Phys. Chem. C* **117**, 25961 (2013).

139. **J.B. Varley, K. Kweon, P. Mehta, P. Shea, T.W. Heo, T.J. Udovic, V. Stavila, and B.C. Wood**: Understanding ionic conductivity trends in polyborane solid electrolytes from ab initio molecular dynamics. *ACS Energy Lett.* **2**, 250 (2017).

140. **K.E. Kweon, J.B. Varley, P. Shea, N. Adelstein, P. Mehta, T.W. Heo, T.J. Udovic, V. Stavila, and B.C. Wood**: Structural, chemical, and dynamical frustration: Origins of superionic conductivity in *closo*-borate solid electrolytes. *Chem. Mater.* **29**, 9142 (2017).

141. **Y. Kato, S. Hori, T. Saito, K. Suzuki, M. Hirayama, A. Mitsui, M. Yonemura, H. Iba, and R. Kanno**: High-power all-solid-state batteries using sulfide superionic conductors. *Nat. Energy* **1**, 16030 (2016).

142. **M. Dimitrievska, P. Shea, K.E. Kweon, M. Bercx, J.B. Varley, W.S. Tang, A.V. Skripov, V. Stavila, T.J. Udovic, and B.C. Wood**: Carbon incorporation and anion dynamics as synergistic drivers for ultrafast diffusion in superionic LiCB$_{11}$H$_{12}$ and NaCB$_{11}$H$_{12}$. *Adv. Energy Mater.* **8**, 1703422 (2018).

143. **M. Kar, O. Tutusaus, D.R. MacFarlane, and R. Mohtadi**: Novel and versatile room temperature ionic liquids for energy storage. *Energy Environ. Sci.* **12**, 566 (2019).

144. **Y. Oumellal, A. Rougier, G.A. Nazri, J.M. Tarascon, and L. Aymard**: Metal hydrides for lithium-ion batteries. *Nat. Mater.* **7**, 916 (2008).

145. **L. Aymard, Y. Oumellal, and J.P. Bonnet**: Metal hydrides: An innovative and challenging conversion reaction anode for lithium-ion batteries. *Beilstein J. Nanotechnol.* **6**, 1821 (2015).

146. **S.G. McArthur, L.X. Geng, J.C. Guo, and V. Lavallo**: Cation reduction and comproportionation as novel strategies to produce high voltage, halide free, carborane based electrolytes for rechargeable Mg batteries. *Inorg. Chem. Front.* **2**, 1101 (2015).

147. **J. Cabana, L. Monconduit, D. Larcher, and M.R. Palacin**: Beyond intercalation-based Li-ion batteries: The state of the art and challenges of electrode materials reacting through conversion reactions. *Adv. Mater.* **22**, E170 (2010).

148. **J.A. Teprovich, J. Zhang, H. Colón-Mercado, F. Cuevas, B. Peters, S. Greenway, R. Zidan, and M. Latroche**: Li-driven electrochemical conversion reaction of AlH$_3$, LiAlH$_4$, and NaAlH$_4$. *J. Phys. Chem. C* **119**, 4666 (2015).

149. **L. Cirrincione, L. Silvestri, C. Mallia, P.E. Stallworth, S. Greenbaum, S. Brutti, S. Panero, and P. Reale**: Investigation of the effects of mechanochemical treatment on NaAlH$_4$ based anode materials for Li-ion batteries. *J. Electrochem. Soc.* **163**, A2628 (2016).